IVYSPRING INTERNATIONAL PUBLISHER

Theranostics

2024; 14(2): 528-546. doi: 10.7150/thno.87739

Research Paper

Targeted modulation of intestinal epithelial regeneration and immune response in ulcerative colitis using dual-targeting bilirubin nanoparticles

Zewei Zhuo[1,2,3†], Kehang Guo[1,4†], Yujun Luo[1,5†], Qi Yang[1†], Huihuan Wu[1,3], Ruijie Zeng[1,6], Rui Jiang[1,3], Jingwei Li[1,2], Rui Wei[1], Qizhou Lian[7,8,9✉], Weihong Sha[1,2,3,6✉], Yuliang Feng[10,11✉], and Hao Chen[1,2,3,6✉]

1. Department of Gastroenterology, Guangdong Provincial People's Hospital (Guangdong Academy of Medical Sciences), Southern Medical University, Guangzhou 510080, China.
2. The Second School of Clinical Medicine, Southern Medical University, Guangzhou, China.
3. School of Medicine, South China University of Technology, Guangzhou 510006, China.
4. Department of Critical Care Medicine, The Fifth Affiliated Hospital of Zhengzhou University, Zhengzhou 450000, China.
5. Department of Gastroenterology, The Third Affiliated Hospital of Sun Yat-Sen University, Guangzhou, 510630, China.
6. Shantou University Medical College, Shantou 515041, China.
7. Faculty of Synthetic Biology, Shenzhen Institute of Advanced Technology, Chinese Academy of Sciences, Shenzhen, China.
8. Cord Blood Bank, Guangzhou Institute of Eugenics and Perinatology, Guangzhou Women and Children's Medical Center, Guangzhou Medical University, Guangzhou, China.
9. State Key Laboratory of Pharmaceutical Biotechnology, The University of Hong Kong, SAR, China.
10. Department of Pharmacology, School of Medicine, Southern University of Science and Technology, Shenzhen, Guangdong, 518055, China.
11. Botnar Research Centre, Nuffield Department of Orthopaedics, Rheumatology and Musculoskeletal Sciences, University of Oxford Old Road, B4495, Headington, Oxford OX3 7LD, UK.

†: These authors contributed equally to this work

✉ Corresponding authors: Prof. Qizhou Lian, E-mail: qz.lian@siat.ac.cn or qzlian@hku.hk; Prof. Weihong Sha, E-mail: shaweihong@gdph.org.cn; Prof. Yuliang Feng, E-mail: fengyl@sustech.edu.cn; Prof. Hao Chen, E-mail: chenhao@gdph.org.cn.

Received: 2023.07.03; Accepted: 2023.11.22; Published: 2024.01.01

Abstract

Rationale: The therapeutic benefits of bilirubin in the treatment of ulcerative colitis (UC) are considerable, whereas the underlying mechanism of bilirubin on UC remains unclear remains unexplored. In addition, the weak hydrophilicity and toxicity have limited its translational applications.

Methods: We have developed a colon dual-targeting nanoparticle, for orally delivering bilirubin through hydrogel encapsulation of hyaluronic acid (HA)-modified poly (lactic-co-glycolic acid) (PLGA) nanoparticles (HA-PLGA$_{Bilirubin}$). Confocal microscopy and *in vivo* imaging were used to evaluate the uptake and the targeted property of HA-PLGA$_{Bilirubin}$ in UC. Immunohistochemistry, immunofluorescence, and transcriptomic analyses were applied to examine the therapeutic effect and potential mechanism of HA-PLGA$_{Bilirubin}$ in UC.

Results: Our results indicated that HA-PLGA$_{bilirubin}$ can significantly enhance the release of bilirubin at simulated intestinal pH and demonstrate higher cellular uptake in inflammatory macrophages. Moreover, *in vivo* biodistribution studies revealed high uptake and retention of HA-PLGA$_{bilirubin}$ in inflamed colon tissue of UC mouse model, resulting in effective recovery of intestinal morphology and barrier function. Importantly, HA-PLGA$_{bilirubin}$ exerted potent therapeutic efficacy against ulcerative colitis through modulating the intestinal epithelial/stem cells regeneration, and the improvement of angiogenesis and inflammation. Furthermore, genome-wide RNA-seq analysis revealed transcriptional reprogramming of immune response genes in colon tissue upon HA-PLGA$_{bilirubin}$ treatment in UC mouse model.

Conclusion: Overall, our work provides an efficient colon targeted drug delivery system to potentiate the treatment of ulcerative colitis via modulating intestinal epithelium regeneration and immune response in ulcerative colitis.

Keywords: ulcerative colitis; bilirubin; targeted therapy; intestinal stem cells; immune response

Introduction

Ulcerative colitis (UC) is a chronic and recurrent gastrointestinal disease [1], dramatically impacts the quality of patients' life. Persistent and diffuse mucosal inflammation episodes, along with dysregulated mucosal immune response, are associated with the pathogenesis of UC [2, 3]. Although the UC patients achieve symptom remission through the use of biologics, steroids, and other immunosuppressive agents [4], long-term administration of these medications may lead to serious complications such as hepatotoxicity, autoimmune diseases, and even malignancy [5-7]. Therefore, there is an urgent need for an advanced therapeutic platform for the treatment of UC.

New candidate agents, such as potent antioxidant drug bilirubin, are being developed and have gained significant attention for their beneficial effects. As a hydrophobic byproduct of heme catabolism, bilirubin has been reported to possess powerful antioxidant effects [8-12] and anti-inflammatory properties [9, 13-15] in intestinal injury disease. Recent studies have also suggested that bilirubin may have immunomodulatory activity in colitis [15, 16], which further extends its clinical and translational value. However, the current understanding of the mechanisms underlying the effects of bilirubin in UC remains largely unexplored, and further investigation is necessary to fully elucidate its therapeutic potential.

Additionally, the hydrophobic nature and toxicity of bilirubin limit its delivery efficacy in vivo and hinder its clinical application [17]. Previous literature has made progress in developing hyaluronic acid (HA)-based bilirubin nanoparticles for the treatment of colitis and acute kidney injury (AKI) [18, 19], demonstrating therapeutic potential in the laboratory. Nevertheless, their uncontrollable systemic diffusion and potential undesirable side effects limit their clinical application through oral administration [20, 21]. Furthermore, gastric proteolytic enzymes and acidic conditions in the gastrointestinal tract (GIT) can cause partial degradation of HA, affecting its effectiveness in UC [22, 23]. One way to overcome these challenges is by introducing a colon-targeted shell that protects HA from GIT degradation while enabling HA-bilirubin nanoparticles to specifically degrade in the colon. Hydrogels (chitosan/alginate) may be suitable candidates for the oral administration delivery of nanoparticles due to their biocompatibility and pH-responsive properties [24], although the introduction of hydrogels into HA-bilirubin nanoparticles has not been explored.

In this study, we aimed to develop a Hydrogel-HA-poly (lactic-co-glycolic acid) (PLGA) system for the oral delivery of bilirubin against UC. The system consists of hydrogel, PLGA, cationic liposome, and HA. The PLGA shell enhances the hydrophilicity of bilirubin, and the cationic liposome facilitates the adsorption of hyaluronic acid through electrostatic interactions, which enhances the targeting ability and therapeutic efficacy of the nanocomplex in inflammatory tissues. Moreover, with the assistance of the hydrogel, the HA-$PLGA_{bilirubin}$ system can be effectively administered through oral gavage to achieve pH-responsive release and target inflamed colon tissues. Importantly, our study reveals novel recovery mechanisms of HA-$PLGA_{bilirubin}$ in UC, including the modulation of colonic epithelial/stem cell regeneration, angiogenesis, and transcriptional reprogramming of immune response genes, thereby expanding our knowledge of the therapeutic mechanisms of bilirubin. The synthetic strategy, targeted delivery system, and histological recovery mechanism of the nanoparticles are summarized in Scheme 1. This study may enhance the bioavailability and therapeutic response of bilirubin, providing an effective oral targeted delivery option for the treatment of UC.

Methods

Preparation of HA-$PLGA_{bilirubin}$

$PLGA_{bilirubin}$ were fabricated using the emulsion-solvent evaporation method as described in previous reports. Briefly, 0.5 mL of PLGA (10 mg/mL), 0.1 mL of cationic liposome DOTAP (20 mg/mL), and 0.05 mL of bilirubin (10 mg/mL) were mixed in a chloroform solution as the organic phase. Then, 5 mL of deionized water was added for sonication in an ice bath for 2 min to generate oil-in-water (O/W) droplets. To remove excess chloroform, the solution was evaporated under rotation after the completion of the reaction. Subsequently, the supernatant containing $PLGA_{bilirubin}$ was recovered by centrifugation for 30 min at 2000 rpm and 4 °C, and the excess free bilirubin was removed. To determine the encapsulation efficacy, the collected $PLGA_{bilirubin}$ was lyophilized, dissolved in DMSO, and the concentration of bilirubin was then measured using a UV–vis–NIR spectrophotometer (Shimadzu UV-2600, Japan). The encapsulation efficiency of bilirubin was calculated as follows:

$$Encapsulation\ efficiency = \left(\frac{weight\ of\ bilirubin\ in\ formulation}{initial\ weight\ of\ bilirubin\ added}\right) * 100\%$$

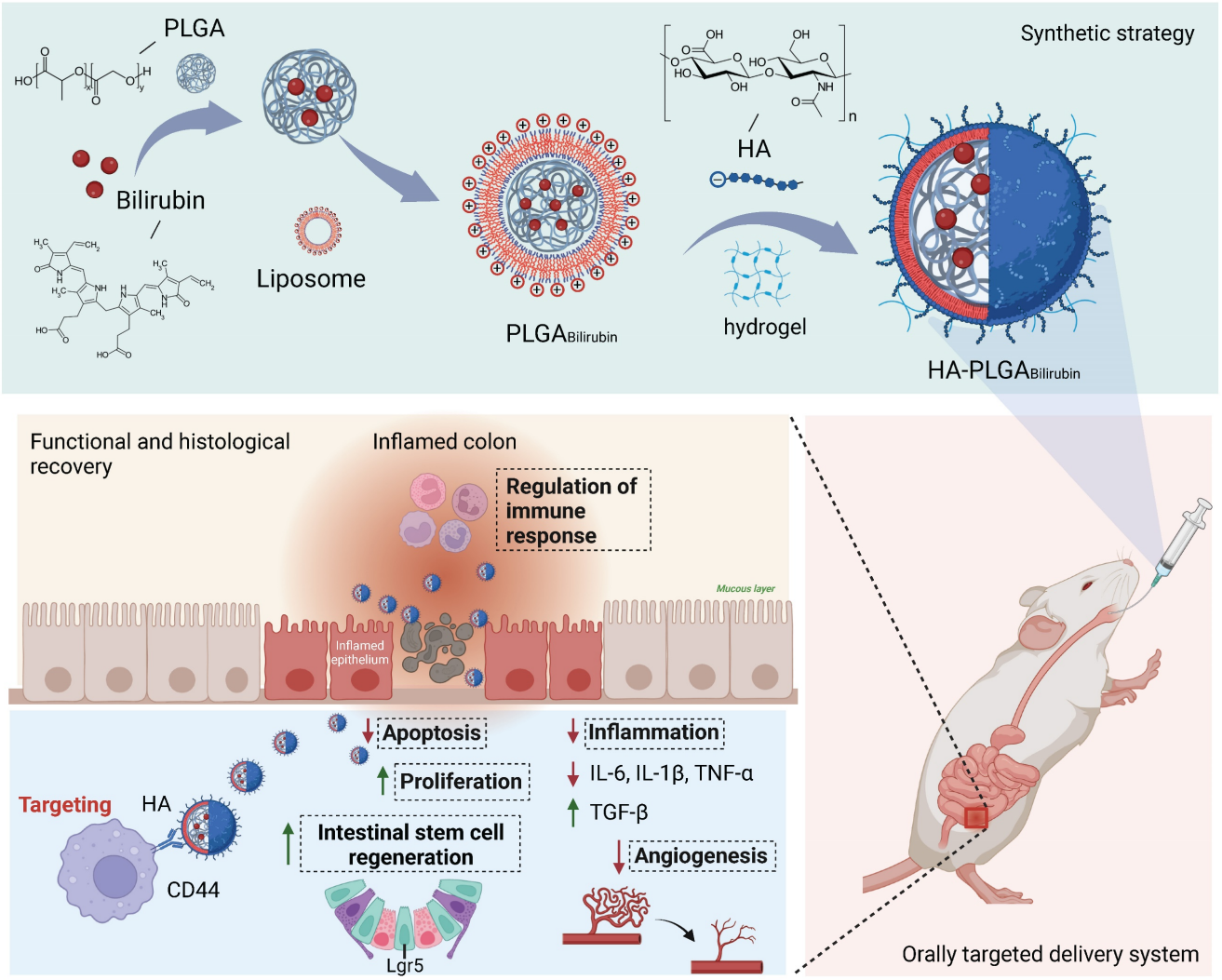

Scheme 1. Schematic design of hydrogel encapsulating hyaluronic acid-modified PLGA nanoparticles (HA-PLGA$_{bilirubin}$) for the targeted treatment of ulcerative colitis.

Afterward, HA solutions were added to the PLGA$_{bilirubin}$ and mixed, followed by centrifugation. HA-PLGA$_{bilirubin}$ were fabricated through self-assembly driven by electrostatic adsorption. To enhance stability, HA-PLGA$_{bilirubin}$ can further cross-link with a hydrogel system to form an oral gel, as previously described [25]. 12 μL of HA-PLGA$_{bilirubin}$, 20 μL of calcium chloride (140 nM), and 8 μL of alginate (7.5 mg/mL) were mixed well and allowed to generate gelation. Blank HA-PLGA-lip nanoparticles were prepared using the same method without the addition of bilirubin.

Characterization

The UV–vis absorption spectrum of free bilirubin and the prepared nanoparticles was measured using a UV–vis–NIR spectrophotometer. The size distribution and zeta potential of above nanoparticles were determined by Dynamic light scattering (DLS, Malvern Nano ZS90, British). The detailed structural analysis of the materials using Fourier Transform Infrared Spectroscopy (FT-IR). The morphology of the nanoparticles was analyzed by transmission electron microscopy (TEM, JEOL-2100, Japan). The Scanning Electron Microscopy (SEM) was used to investigate the particle size and morphology of HA-PLGA$_{Bilirubin}$ hydrogel under different pH conditions, including simulated colonic fluid (SCF, PH=7.4), simulated intestinal fluid (SIF, pH 6.5), and simulated gastric fluid (SGF, PH=1.2). Scanning Electron Microscopy with Energy Dispersive X-ray Spectroscopy (SEM-EDS) was used to confirm that bilirubin was loaded inside the hydrogel.

In vitro drug release

In vitro drug release experiments were conducted in modified enzymatic pH buffer media using simulated gastrointestinal fluids, as previously described [26]. HA-PLGA$_{bilirubin}$ hydrogel was added to 1 mL of simulated gastrointestinal fluid (SGF, pH=1.2), simulated intestinal fluid (SIF, pH=6.5), and simulated colon fluid (SCF, pH=7.4) at 0, 20, 40, 60,

120, 180, 240, and 300 min. After centrifugation at 2000 rpm, the supernatant containing nanoparticles was collected and subsequently lyophilized. Chloroform solution was added to dissolve the nanoparticles, and the concentration of free bilirubin was quantified by measuring its absorbance under ultraviolet light in a microplate. To observe the impact of hydrogel and non-hydrogel at different pH conditions on drug release, nanoparticles encapsulated in hydrogel and nanoparticles encapsulated in non-hydrogel were placed separately in SGF, SIF, and SCF at time points of 0 min, 60 min, and 180 min, respectively. The subsequent steps remain the same as before.

Cellular uptake

The cellular uptake of HA-PLGA$_{bilirubin}$ was analyzed using fluorescence-activated cell sorter (FACS) and confocal laser scanning microscopy (CLSM, Nikon E-A1, Japan). To mimic an inflammatory state, RAW 264.7 macrophages were treated with 100 μg of LPS and 10 μg of INF-r in serum-free conditions to induce a M1 phenotype. After 24 h of induction, DID-loaded nanoparticles were added to the cells for 4 h in serum-free conditions, and flow cytometry was performed to assess the uptake of the DID-loaded nanoparticles. The experimental method involved assessing the percentage of cells containing DID-loaded nanoparticles by establishing a cutoff fluorescence intensity derived from a histogram of control cells. Subsequently, the uptake of the DID-loaded nanoparticles by M1-induced RAW 264.7 macrophages was observed using CLSM. Alexa Fluor 488 phalloidin and DAPI were used to stain the membrane and nucleus of the cells, respectively.

3-(4,5-dimethylthiazol-2-yl)-2,5-diphenyltetrazolium bromide (MTT) assay

Cells were initially inoculated into a 96-well plate, left to adhere overnight. For each well, add 20 μl of MTT solution and incubate for 4 h. Terminate the culture, and carefully remove the culture supernatant. Add 150 μl of DMSO to each well, and shake for 10 min to ensure complete dissolution of the crystals. Measure the optical density of each well at 490 nm using an enzyme-linked immunosorbent assay reader and record the results.

Construction of mimic UC animal model

Six-week-old C57/BL/6 mice were purchased from Guangdong Medical Laboratory Animal Center. Animal care and experiments were carried out in accordance with and approved by the Ethics Review Committee of Guangdong Provincial People's Hospital (KY-Z-2021-021). All mice were acclimatized for one week and then randomly assigned to different treatment groups. To induce the colitis model, mice were provided with drinking water containing 3% Dextran Sulfate Sodium Salt (DSS) for 5-6 days, followed by normal water for 4-5 days. Healthy mice were given only normal water as a control group. The DSS-induced mice were randomly divided into five groups (3-5 mice per group), and then administered with 30 mg/kg of bilirubin [18], HA-PLGA-lip, PLGA$_{bilirubin}$ (equivalent mass of bilirubin as in 30 mg/kg bilirubin), and HA-PLGA$_{bilirubin}$ (equivalent mass of HA-PLGA-lip and bilirubin) were dosed on predetermined days via oral gavage. Body weight was measured daily and the disease activity index (DAI) was determined to quantify colitis severity and the degree of improvement as previously stated. After cessation of various treatment, mice were sacrificed by decapitation and the colon length was measured from cecum to anus and photographed for preservation. The colon tissue specimens of the distal section were harvested for hematoxylin and eosin (HE) and immunofluorescence staining. The remaining colon tissues were snap frozen and stored at -80 °C for transcriptome sequencing analysis and the concentrations of cytokines and MPO level detection.

In vivo biocompatibility evaluation

Six-week-old C57/BL/6 mice were orally treated with saline (control) or HA-PLGA$_{bilirubin}$ (30 kg/mL) for 7 days. Blood was collected from the retroorbital region of mice for biochemical indicators detection, and their organs (heart, liver, spleen, lungs, and kidneys) were removed for histopathological analysis after cervical dislocation. The following hematology values were determined by an automated hematology analyzer (model XT-2000iV, Sysmex, Lincolnshire, IL): alanine aminotransferase (ALT), aspartate aminotransferase (AST), Alkaline Phosphatase (ALP), UREA, Total Protein (TP), red blood cells (RBC), white blood cells (WBC), platelet (PLT), mean corpuscular hemoglobin (MCH), mean corpuscular volume (MCV). Fixed organs were embedded in paraffin and 4% buffered formalin and 70% alcohol. Sections were stained with H&E and examined under a microscope.

Rhodamine-(Rho) and Cy5.5 labeled HA-PLGA$_{Bilirubin}$

Rhodamine-N-hydroxy succinimide (Rho-NHS) or Cy5.5-NHS was prepared at a 1:100 molar ratio to HA-PLGA$_{Bilirubin}$. In brief, Rho-NHS or Cy5.5-NHS and EDC (1.2 equiv) were combined and stirred in 2 mL of DMSO for 20 min at room temperature in the absence of light. Following this, 1 mg/mL HA-PLGA$_{Bilirubin}$ was introduced. After allowing this reaction mixture to proceed for 2 h at room

temperature, any unreacted Rho-NHS or Cy5.5-NHS was eliminated via dialysis for up to 12 h using molecular-porous membrane tubing. This was followed by three precipitations with acetone and the end product underwent lyophilization.

Biodistribution

To evaluate the biodistribution of nanoparticles in the colon, normal and DSS-induced mice were orally treated with Cy5.5-labeled HA-PLGA$_{Bilirubin}$, Bilirubin, PLGA$_{Bilirubin}$, and HA-PLGA$_{Bilirubin}$. After oral delivery, mice were imaged using an AniView100 small animal living imaging system (BLT, China) at 4, 8, and 24 h. After 24 h, mice were sacrificed, and the heart, liver, spleen, lung, kidney, and colon were harvested for *ex vivo* imaging. Fluorescence intensity detection was analyzed using AniView100 Living Imaging software from BLT company. *In vivo* pharmacokinetic assessments were conducted using noncompartmental methods [27] to determine the maximum observed plasma concentrations (Cmax) and areas under the plasma concentration-time curve (AUC) from 0 to 72 h after various treatments.

Flow Cytometry

The colon tissue was digested into a single-cell suspension. Subsequently, the following extracellular antibodies were added: Recombinant Alexa Fluor® 488 anti-EpCAM Antibody, Recombinant APC anti-Ly6G Antibody, PerCP/cyanine 5.5-conjugated anti-F4/80 Antibody, phycoerythrin (PE)-conjugated anti-CD11c Antibody, and Brilliant Violet 605™ anti-CD11b Antibody. The cells were incubated at room temperature in the dark for 30 min to immunostain cell surface markers. After surface molecule staining, the cells were resuspended in fixation/permeabilization solution and incubated in the dark for 15 min. Flow cytometry analysis was performed using a BD Celesta system, and the data were analyzed using FlowJo software.

HE staining

A 4% paraformaldehyde solution was used to fix the colon tissues, followed by embedding them in paraffin. The paraffin-embedded specimens were then cut into 5 μm thick sections. Deparaffinization of the sections was performed using xylene, followed by hydration with gradient alcohol according to standard procedures [28]. After washing the sections with distilled water, the nucleus of the sections was stained with hematoxylin for 10-15 min, followed by counterstaining with eosin for 2-5 min. Tissue morphology, including mucosal architecture changes, infiltration of inflammatory cells, goblet cell numbers, villus height, alterations in crypt drop out, and surface epithelial cell hyperplasia, was observed under light microscopy to evaluate the degree of intestinal mucosa damage and recovery in a double-blinded manner.

Intestinal permeability assessment

Intestinal permeability assay was performed to assess the intestinal barrier functions of these mice through oral administration of 4 kDa FITC-dextran, as previously described [18]. Briefly, mice with various treatment were fasted for 4 h, followed by oral administration of FITC-dextran (0.6 mg per gram of body weight). After 3 h, blood samples were collected via retro-orbital bleed, and the levels of FITC-dextran in the blood were measured using fluorescence, with excitation at 485 nm and emission at 520 nm.

Immunohistochemical staining

After deparaffinization and hydration following the above procedures, tissue sections were subjected to antigen retrieval using 10 mM citrate acid under high pressure for 20 min. Subsequently, the sections were blocked with 10% goat serum for 60 min. After washing with a wash buffer, primary antibodies against PCNA (#13110, Cell Signaling Technology (CST)) were added to the sections and incubated overnight at 4 °C. Following this, the sections were incubated with biotin-labeled secondary antibodies for 30 min at 37 °C, followed by incubation with streptavidin-coupled horseradish peroxidase (HRP) for an additional 30 min at 37 °C. Color development was achieved using diaminobenzidine (DAB) chromogen for 3 min, and hematoxylin was finally used as a counterstain for 2-3 s. PCNA-positive nuclei in the crypt were visualized under a light microscope after the immunohistochemical procedures.

Immunofluorescence staining

The tissue sections were deparaffinized, hydrated, subjected to antigen retrieval, and blocked with 10% donkey serum following the above procedures. For CD31 staining, primary antibodies against CD31 (1:1000, Company) were incubated overnight at 4 °C. The next day, the sections were incubated with a fluorescence secondary antibody, Alexa Fluor®594 donkey anti-rat IgG (H+L) (1:400, Life Technologies, A21209), for 30 min at 37 °C. After rinsing with tris buffered saline (TBS), the sections were stained with DAPI solution (Roche, 216276) for nuclear staining. The sections were then sealed with an anti-fluorescence quencher and observed under a darkfield microscope.

TUNEL staining

TUNEL staining was performed using the In Situ TUNEL Detection Kits (Roche Diagnostics GmbH). According to the manufacturer's instructions, tissue

sections were pretreated and incubated with Proteinase K working solution for 15-30 min at 37 °C. After washing, the TUNEL reaction mixture was added and incubated for 60 min at 37 °C in a humidified and dark environment. DAPI solution was applied to stain the nuclei, and then the sections were analyzed under a fluorescence microscope.

Enzyme-Linked Immunosorbent Assay (ELISA) analysis

ELISA kits for MPO, VEGF-A, TGF-β, IL-4, IL-1β, IL-6, TNF-α, and IFN-γ were purchased from CUSABIO company. According to the manufacturer's instructions, colon tissues were broken into small pieces and homogenized in PBS solution using a tissue homogenizer. After centrifugation at 5000 x g for 5 min at 4 °C, the supernatants were collected and stored at -20 °C or -80 °C.100 µl of standard and sample were added to each well and incubated for 2 h at 37 °C. After removing the liquid, 100 µl of Biotin-antibody (1x) was added to each well and incubated for 1 h at 37 °C. After washing, 100 µl of HRP-avidin (1x) was added to each well and incubated for 1 h at 37 °C. 90 µl of TMB Substrate was added to each well and incubated for 15 min at 37 °C in the dark. Then, 50 µl of Stop Solution was added to each well and incubated for 5 min. OD values were measured using a microplate reader at a wavelength of 450 nm, and standard curves were established to measure the concentrations of MPO, VEGF-A, TGF-β, IL-1β, IL-6, and TNF-α in each sample.

Quantitative reverse transcription polymerase chain reaction (qRT-PCR)

Colon tissue was isolated from the intestinal tract and stored at -80 °C to prevent RNA degradation. Total RNA from the cells was extracted using the E.Z.N.A. Total RNA Isolation Kit (Omega, GA, USA). Reverse transcription to generate cDNAs was performed using the PrimeScript™ RT-PCR kit (TaKaRa, Otsu, Japan). Following the manufacturer's instructions for the Biorad CFX Connect (Bio-Rad Laboratories, CA, USA), quantitative real-time polymerase chain reaction (qRT-PCR) was carried out using SYBR Premix Ex Taq (TaKaRa, Otsu, Japan). The specific steps for qRT-PCR were conducted as previously described [29] to quantitatively measure the relative mRNA levels of tight junction-related genes (ZO-1 and Ocludin-1). The specific primer sequences used were as follows: ZO-1, 5′-CCA GCA ACT TTC AGA CCA CC-3′ (forward) and 5′-TTG TGT ACG GCT TTG GTG TG-3′ (reverse); Ocludin-1, 5′-GCT TAC AGG CAG AAC TAG ACG-3′ (forward) and 5′-TCT GCA GAT CCC TTA ACT TGC-3′ (reverse); β-actin, 5′-ATG GAA TCC TGT GGC ATC CAT-3′ (forward) and 5′-TCC TGC CATC CTG TCA GCA ATG-3′ (reverse).

Western Blot

As the previous study described [30], proteins are extracted, separated on an SDS-PAGE gel, and transferred to a membrane. After blocking with 5% non-fat milk, the membrane is probed with a primary antibody specific to the target protein, followed by incubation with a secondary antibody. Washing steps remove unbound antibodies. The target protein is visualized using chemiluminescence, and its levels are quantified.

Transcriptome sequencing analysis

As stated above, colon tissues were harvested from the following groups: normal mice group (Control), DSS-induced mice treated with PBS group (DSS), DSS-induced mice treated with $PLGA_{bilirubin}$ (DSS+$PLGA_{bilirubin}$), and DSS-induced mice treated with HA-$PLGA_{bilirubin}$ (DSS+HA-$PLGA_{bilirubin}$). The samples were stored at -80 °C, and RNA extraction and transcriptome sequencing analysis were performed. Data processing was conducted using Novomagic (https://magic.novogene.com).

Statistical analysis

A statistical analysis was performed using Prism software (GraphPad Prism). Students t-test or Welch's t-test were used to analyze continuous variables. Statistical significance was considered at a *p*-value less than 0.05.

Results

Preparation and characterization of HA-$PLGA_{bilirubin}$

We synthesized hydrogel-encapsulating HA-modified PLGA nanoparticles for the delivery of bilirubin (HA-$PLGA_{bilirubin}$) using the double emulsion-solvent evaporation method and electrostatic adsorption interaction. The synthesis process is described in Figure 1A. The chloroform containing the mixture was removed by rotary evaporation to allow bilirubin to transfer to the PLGA hydrophobic core through the 'like dissolves like' principle. The half-width of the absorption peak broadened when the bilirubin was successfully coated with 1,2-dioleoyl-3-trimethylammonium-propane (DOTAP) and PLGA nanoparticles (Figure 1B). This change is probably because these substances interacted with each other, which caused the size range to increase [31] and affected the Localized Surface Plasmon Resonance (LSPR) [32], which, in turn, resulted in a broader peak in the absorption spectrum. Quantification of bilirubin loading in the

DOTAP-PLGA nanoparticles was performed using UV to measure the drug loading yield and efficiency (Figure 1C). The bilirubin concentration was calculated to be 23.8±1.3 μg/mL based on the standard curve (Figure S1). According to the formulation of encapsulation efficiency, the encapsulation efficiency of bilirubin into DOTAP-PLGA nanoparticles was 47.6±2.7%, determining the effectiveness of the PLGA nanoparticles in entrapping the bilirubin. The nanoparticles were then characterized for size and zeta potential at each coating stage. The average particle size of $PLGA_{Bilirubin}$ eventually stabilized at 163.91±1.96 nm, and the zeta potential stabilized at 53.26±2.73 mV by increasing the feeding of DOTAP (Figure S2; Figure S3). As HA is a negatively charged polysaccharide, it can be modified on the surface of $PLGA_{bilirubin}$ by electrostatic adsorption, which is attributed to the cationic properties of cationic liposomes. When the $PLGA_{Bilirubin}$ was modified with HA, the zeta potential decreased from 49.71±1.63 mV to 24.86±2.55 mV (Figure 1D), and the average particle size increased from 156.83±17.23 nm to 193.23±12.85 nm (Figure 1E). The polydispersity indices (PDIs) of the $PLGA_{Bilirubin}$ and HA-$PLGA_{Bilirubin}$ were <0.2, highlighting their narrow size distribution (Table S1). In fact, while DOTAP holds promise for delivering hydrophobic drugs [33-36], its highly positive charge can still pose issues related to hemolysis [37, 38]. Here, we use the electrostatic adsorption of HA onto DOTAP liposomes to prepare HA-targeted nanoparticles. This approach helps neutralize the toxicity associated with cationic liposomes [39] and, by adsorbing HA, enables bilirubin nanoparticles to target CD44 ligands highly expressed in inflamed tissues [40]. Transmission Electron Microscopy (TEM) images demonstrated that $PLGA_{Bilirubin}$ and HA-$PLGA_{Bilirubin}$ were vesicle-like nanoparticles with mean diameters of ~80 nm and ~120 nm, respectively (Figure 1F). Next, we conducted detailed structural analysis of the materials using Fourier Transform Infrared Spectroscopy (FT-IR) (Figure S4). The peaks at approximately 3407 cm^{-1} signify the existence of O-H functional groups. A distinctive absorption band at around 3420 cm^{-1} is observed in HA-$PLGA_{Bilirubin}$, which correspond to their presence of multiple hydroxyl groups. The peaks observed in the range of 1693-1746 cm^{-1} are associated with the stretching vibrations of C=O bonds in the three different nanoparticles. Additionally, the peak at 1047 cm^{-1} can be attributed to the C-N stretching vibrations on $PLGA_{Bilirubin}$ and HA-$PLGA_{Bilirubin}$. Furthermore, the 1091 cm-1 peak corresponds to the stretching vibrations of ether bonds, which are present in $PLGA_{Bilirubin}$ and HA-$PLGA_{Bilirubin}$ but absent in Bilirubin. These results clearly indicate the structural distinctions between the three nanomaterials. In addition, after incubating the HA-$PLGA_{Bilirubin}$ nanoparticles in both Phosphate-Buffered Saline (PBS) and Fetal Bovine Serum (FBS) for 8 days, their size remained essentially unchanged, demonstrating excellent stability in FBS (Figure S5).

Uptake and drug release of HA-$PLGA_{bilirubin}$

The controllable release of bilirubin from HA-$PLGA_{bilirubin}$ to the colonic tissues under specific pH conditions is critical for improving the bioavailability of the drug. Herein, we encapsulated the nanoparticles into a hydrogel composed of chitosan and alginate and observed the release of bilirubin in simulated gastrointestinal conditions. As shown in Figure 2A, the release of bilirubin at pH 7.4 (simulated colonic fluid, SCF) was higher than that at pH 1.2 (simulated gastric fluid, SGF), and slightly higher than PH 6.8 (simulated intestinal fluid, SIF). In addition, our results demonstrate that in simulated gastric fluid (SGF), nanoparticles without hydrogel encapsulation (HA-$PLGA_{Bilirubin}$) achieved a release of 54.56%, which was 45.17% higher than that of HA-$PLGA_{Bilirubin}$ hydrogel. HA-$PLGA_{Bilirubin}$ within the hydrogel started substantial bilirubin release in SIF and gradually stabilized in SCF. These results clearly confirm the pH-responsive properties of the hydrogels (chitosan/alginate) for drug release (Figure S6). Furthermore, we conducted Scanning Electron Microscopy with Energy Dispersive X-ray Spectroscopy (SEM-EDS) analysis on both bilirubin and the HA-$PLGA_{Bilirubin}$ hydrogel. As shown in Figure S7, the SEM-EDS results clearly demonstrate the composition of the materials. We found that carbon (C), nitrogen (N), and oxygen (O) are the primary elements in bilirubin. However, following the encapsulation of bilirubin within the hydrogel, we observed the appearance of calcium (Ca) and chlorine (Cl) components, accompanied by a decrease in the relative proportions of C, N, and O. This observation serves as supportive evidence that bilirubin was indeed loaded inside the hydrogel. The pH responsiveness of the hydrogel is attributed to the protonation and deprotonation of functional groups on the sodium alginate backbone and crosslinking agents, which result in changes in the polymer conformation and swelling behavior. Specifically, sodium alginate is a pH-sensitive, anionic polysaccharide that undergoes structural changes in response to pH variations. In acidic environments (e.g., stomach), the carboxyl groups in sodium alginate become protonated (–COOH), leading to a reduction in repulsive forces between the polymer chains.

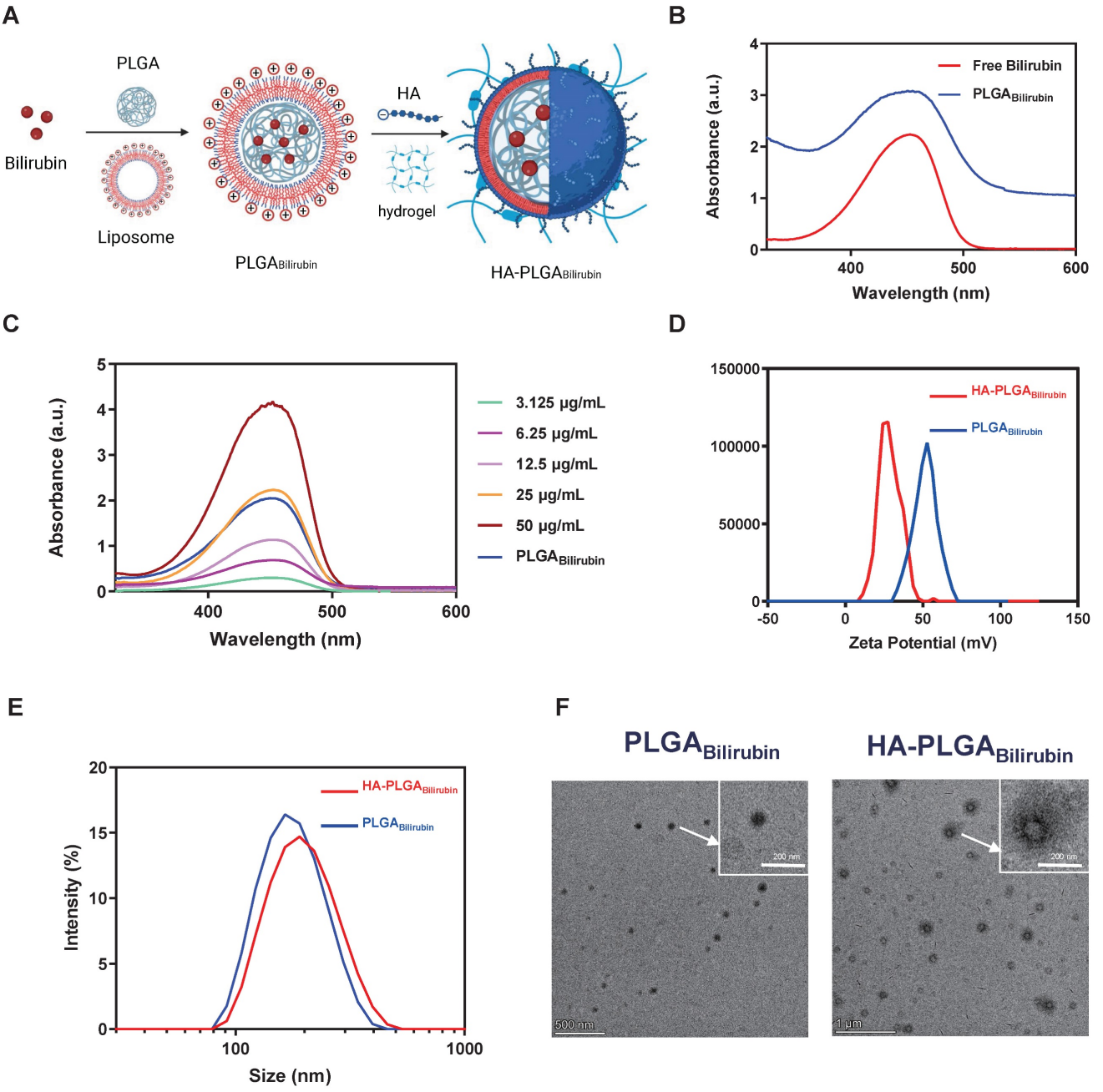

Figure 1. Preparation and characterization of HA-PLGA$_{bilirubin}$. (A) Schematic design of the preparation of HA-PLGA$_{bilirubin}$. (B) Absorption spectrum of PLGA$_{Bilirubin}$. Absorptive peak becomes wide when the bilirubin was encapsulated into PLGA nanoparticles. (C) Drug-loading capacity of PLGA$_{Bilirubin}$. The concentration of bilirubin in PLGA$_{Bilirubin}$ was 23.8±1.3 μg/mL, and the drug encapsulation efficiency of PLGA$_{Bilirubin}$ was 47.6±2.7%. (D) Zeta potential of HA-PLGA$_{Bilirubin}$ and PLGA$_{Bilirubin}$. (E) Size distribution of HA-PLGA$_{Bilirubin}$ and PLGA$_{Bilirubin}$. (F) Transmission electron microscopic (TEM) images of HA-PLGA$_{Bilirubin}$ and PLGA$_{Bilirubin}$.

This protonation allows the polymer chains to interact more strongly, resulting in the formation of a compact structure or "gel" that can withstand the harsh acidic conditions. Conversely, in more neutral to alkaline environments (e.g., the colon), the carboxyl groups lose their protons, transitioning to their anionic form (–COO-). This deprotonation increases electrostatic repulsion between polymer chains, causing the hydrogel to swell and disintegrate, thereby releasing the entrapped bilirubin. This pH-responsive behavior of sodium alginate facilitates the targeted delivery of bilirubin to the colonic area, where the conditions trigger gel disintegration and drug release. Additionally, the internal morphology and size of the hydrogel in media with SCF, SGF, and SIF were examined (Figure S8). Our result showed that the cross-sectional morphology appears highly compact at pH 1.2, whereas it becomes more porous and is suitable for drug release in higher pH buffer solutions. The hydrogel particle size increases in the high pH buffer solutions, and surface cracks and collapses begin to appear especially at pH 7.4. This

demonstrates that HA-PLGA$_{bilirubin}$ with hydrogel exhibits good pH sensitivity and can protect bilirubin in SGF and subsequently release it in SCF, exhibiting excellent pH sensitivity and controlled-release performance. Furthermore, to evaluate whether HA-PLGA$_{bilirubin}$ improves the targeting ability of bilirubin toward inflamed colon via HA, we investigated the cellular uptake of the nanoparticles by Lipopolysaccharide (LPS)-treated macrophages (*in vitro* inflammatory model). After incubating the cells with free 1,1'-dioctadecyl-3,3,3',3'-tetramethylindodicarbocyanine perchlorate (DID), DID-PLGA$_{bilirubin}$, and DID-HA-PLGA$_{bilirubin}$ for 4 h, fluorescence-activated cell sorter (FACS) analysis was used to determine the intracellular fluorescence intensity of DID (Figure 2B). It was found that the internalization of DID-HA-PLGA$_{bilirubin}$ was approximately 1.69-fold higher than DID-PLGA$_{bilirubin}$ (Figure 2C). Raw 264.7 macrophages treated with DID-HA-PLGA$_{bilirubin}$ exhibited noticeably higher intracellular fluorescence intensity than cells treated with DID-PLGA$_{bilirubin}$ (p<0.0001, Figure 2D).

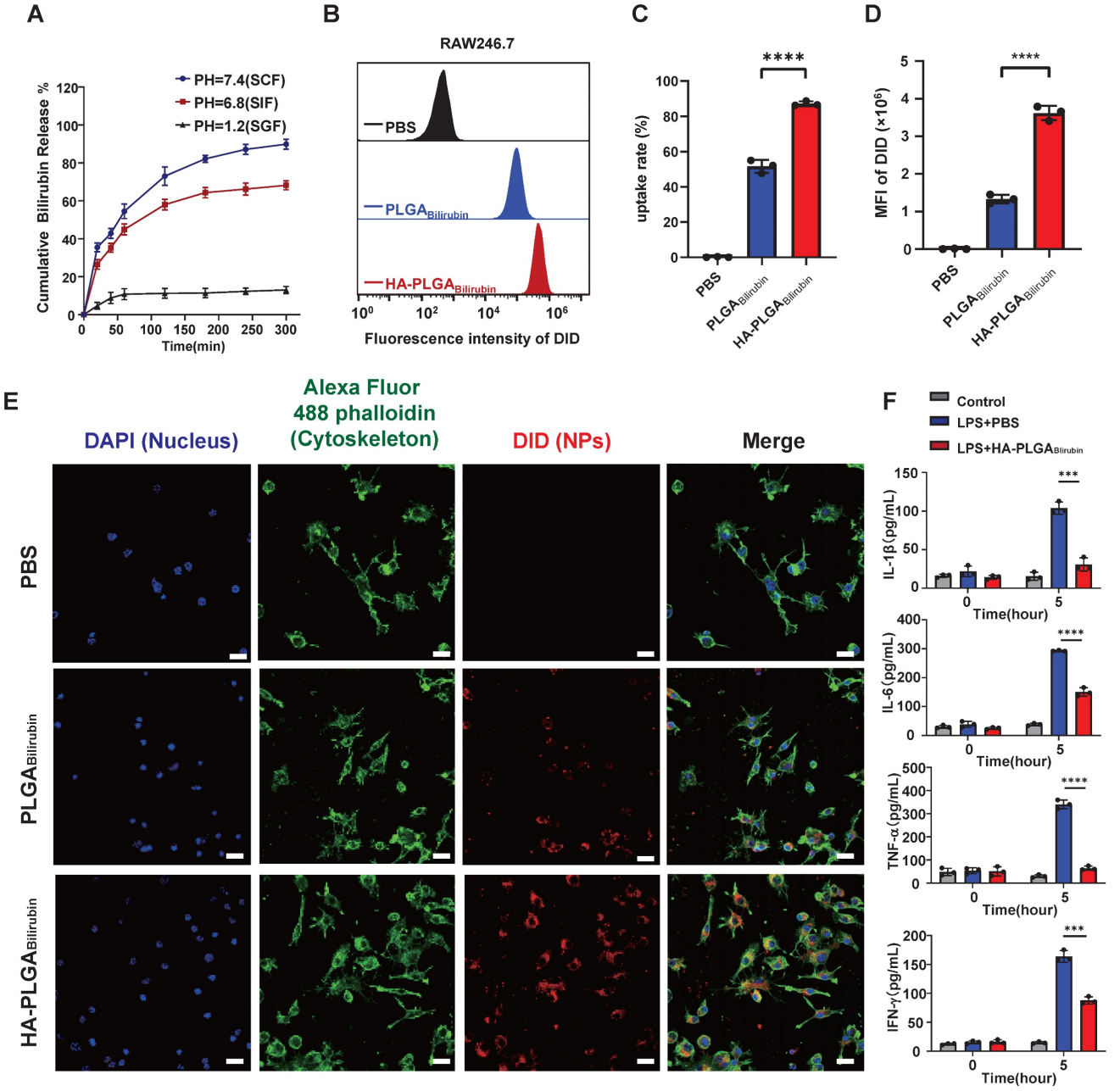

Figure 2. Drug release, cellular uptake and pro-inflammatory cytokines downregulation of HA-PLGA$_{bilirubin}$. (A) Cumulative drug release profile of bilirubin in simulated gastrointestinal pH buffer media. (B) Flow cytometry histograms of uptake of PLGA$_{bilirubin}$ and HA-PLGA$_{bilirubin}$ by Raw 264.7 macrophages. (C) Cellular uptake percentages of PBS, PLGA$_{bilirubin}$ and HA-PLGA$_{bilirubin}$ by RAW 264.7 macrophages. (D) Mean fluorescent intensity (MFI) of Raw 264.7 macrophages treated with PLGA$_{bilirubin}$ and HA-PLGA$_{bilirubin}$. ****represents p<0.0001. (E) Confocal laser scanning microscopy (CLSM) image of RAW 264.7 macrophages treated with PLGA$_{bilirubin}$ and HA-PLGA$_{bilirubin}$. Scale bar, 20μm. (F) Relative protein levels of pro-inflammatory cytokines (IL-1β, IL-6, TNF-α, and IFN-γ) in LPS-induced RAW 264.7 macrophages.

The introduction of HA can potentially modulate the interaction of the nanoparticles with macrophages, altering the uptake dynamics and, consequently, enhancing the fluorescent signal intensity [41]. Confocal laser scanning microscopy (CLSM) images also validated the enhanced cellular uptake performance (increasing red fluorescence signals) in HA-PLGA$_{bilirubin}$ compared to PLGA$_{bilirubin}$ (Figure 2E). Furthermore, we have investigated the impact of HA-PLGA$_{Bilirubin}$ treatment on the secretion of cytokines in LPS-treated Raw 264.7 macrophages. Our findings demonstrated a significant upregulation of major pro-inflammatory cytokines (Interleukin-1 Beta (IL-1β), Interleukin-6 (IL-6), Tumor Necrosis Factor Alpha (TNF-α), and Interferon-Gamma (IFN-γ)) induced by LPS treatment. However, this effect was substantially attenuated by HA-PLGA$_{Bilirubin}$ treatment (Figure 2F). These results suggest that HA-PLGA$_{Bilirubin}$ is readily taken up by LPS-activated macrophages and has the capacity to downregulate their pro-inflammatory responses by suppressing the release of pro-inflammatory cytokines.

Biosafety evaluation of HA-PLGA$_{bilirubin}$

A good biosafety is one of the primary prerequisites for nanomaterials used in biomedical applications. *In vitro*, we have conducted cytotoxicity assays using different nanoparticles, including Bilirubin, HA-PLGA-Lip, PLGA$_{Bilirubin}$, and HA-PLGA$_{Bilirubin}$, at concentrations ranging from 0.1 μg/ml to 100 μg/ml on human intestinal epithelial cells (Caco2) and mouse macrophage cells (Raw 264.7) for a 24 h incubation period. The results of the MTT assay demonstrated that none of the tested nanoparticles exhibited significant cytotoxicity. *In vivo*, we investigated the systemic toxicity of the HA-PLGA$_{bilirubin}$ by blood biochemical index detection and histological assessment of major organs. After various treatment for 3 weeks, function indexes of liver and kidney, such as Alanine Aminotransferase (ALT), Aspartate Aminotransferase (AST), Alkaline Phosphatase (ALP), UREA, and Total Protein (TP), did not change significantly, suggesting that oral administration of the nanoparticles did not impair liver and renal function (Figure S9A-B). Furthermore, there were no significant changes in the level of hematological indexes, such as Red Blood Cells (RBC), Red Blood Cells (WBC), Platelets (PLT), Mean Corpuscular Hemoglobin (MCH), and Mean Corpuscular Volume (MCV) (Figure S9C). Additionally, Hematoxylin and Eosin (HE) staining was used to stain the sections of major organs (heart, liver, spleen, lungs, kidneys) and the histological results revealed no evidence of toxic effects, indicating the high biosafety of HA-PLGA$_{bilirubin}$ (Figure S10).

In vivo biological distribution of HA-PLGA$_{bilirubin}$

To assess the targeting ability of HA-PLGA$_{bilirubin}$, the accumulation ability of HA-PLGA$_{bilirubin}$ on inflamed intestinal regions was then directly tested, and their biodistribution data was measured using the *In Vivo* Imaging System (IVIS) fluorescence intensities (Figure 3A). Cy5.5 was used to label the free bilirubin and nanoparticles, and normal mice were treated with HA-PLGA$_{bilirubin}$ and Dextran Sulfate Sodium Salt (DSS)-induced mice were treated with bilirubin, PLGA$_{bilirubin}$, and HA-PLGA$_{bilirubin}$. Due to the protective effect of the hydrogel, there were still strong fluorescence signals at 4h in the normal mice and DSS-induced mice treated with PLGA$_{bilirubin}$, and HA-PLGA$_{bilirubin}$, whereas the free DSS-induced mice treated with bilirubin showed decreasing fluorescence. With the extension of time, the fluorescence of normal mice and DSS-induced mice treated with PLGA$_{bilirubin}$ was significantly decreasing, whereas the DSS-induced mice treated with HA-PLGA$_{bilirubin}$ still had a strong fluorescence signal at 12h and 24h. After 24h, DSS-induced mice treated with the same dose of HA-PLGA$_{bilirubin}$ had a significantly higher fluorescence intensity than that of normal mice (~5.46-fold). Furthermore, orally-administered HA-PLGA$_{bilirubin}$ showed at least 8.64-fold and 5.57-fold level of accumulation in DSS-induced mice compared to bilirubin and PLGA$_{bilirubin}$, respectively (Figure 3C). The result of the *ex vivo* fluorescence images of major organs is consistent with the result of *in vivo* images (Figure 3D). Orally-administered HA-PLGA$_{bilirubin}$ exhibited the strongest accumulation (~6.24-fold) in inflame colon tissue compared to PLGA$_{bilirubin}$ (Figure 3E), indicating that PLGA$_{bilirubin}$ bearing HA ligands could significantly enhance the accumulation of bilirubin in the colitis tissues. *In vivo* pharmacokinetic studies further demonstrated that HA-PLGA$_{bilirubin}$ formulation could increase the C_{max} of bilirubin by about 6.69-fold and overall increase in the oral bioavailability by approximately 5.24-fold when compared to the free bilirubin (Figure 3F). Furthermore, we performed fluorescence microscopy on colon tissue sections from DSS-induced colitis mice that had been orally administered Rhodamine (Rho)-HA-PLGA$_{Bilirubin}$. The results demonstrated substantial uptake of the nanoparticles by the inflame colon tissues, and Rho-HA-PLGA$_{Bilirubin}$ exhibited colocalization with macrophages expressing F4/80 (Figure 3G).

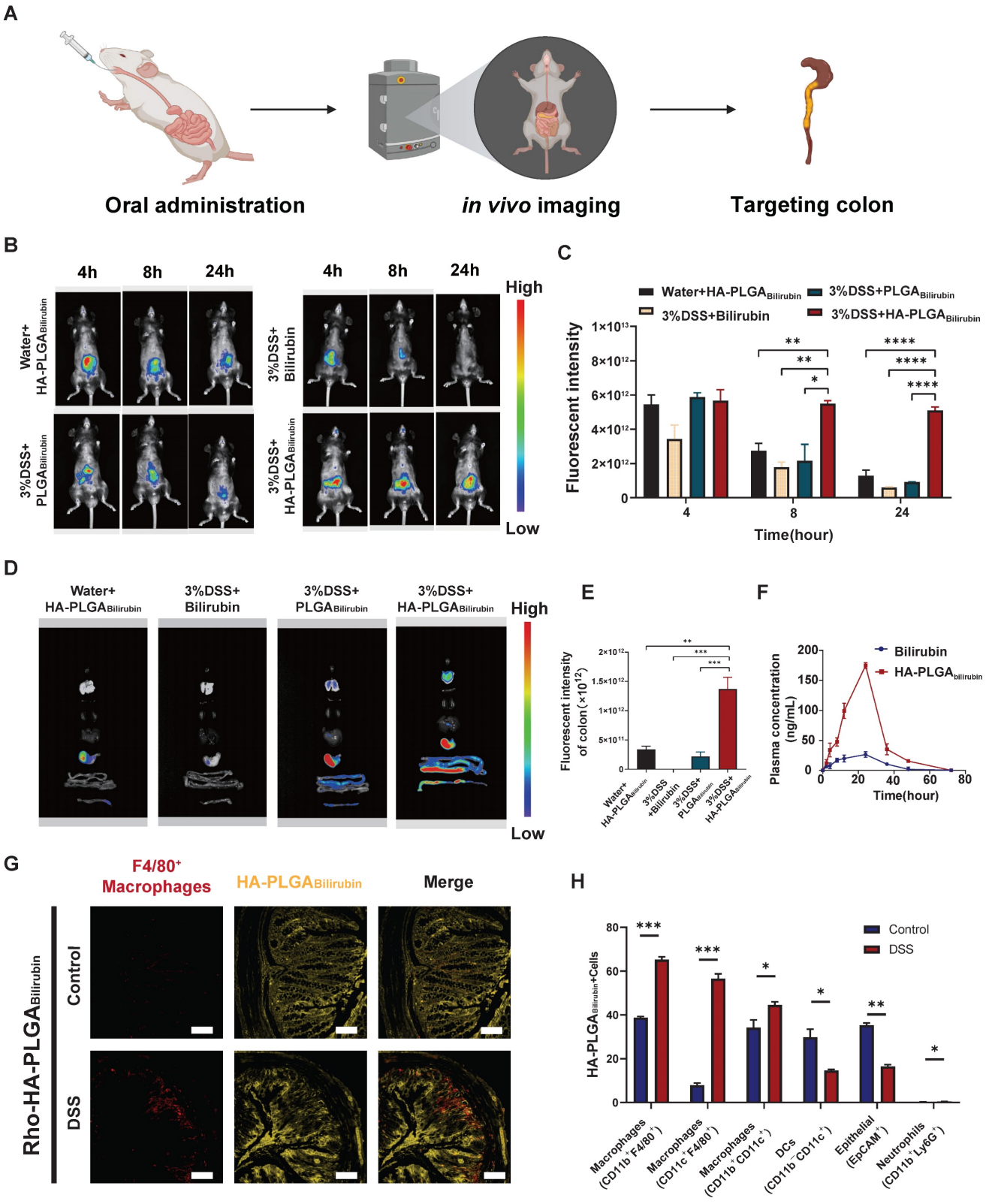

Figure 3. Orally administered HA-PLGA$_{bilirubin}$ specifically targets the inflamed colon of DSS-induced mice. (A) Schematic representation of *in vivo* imaging for the DSS-induced mice. (B) Representative images of *in vivo* fluorescence imaging of treating animals with Bilirubin, PLGA$_{Bilirubin}$, or HA-PLGA$_{Bilirubin}$, after 4h, 8h, 24h. (C) Quantification for *in vivo* fluorescence signal at different time-points after various treatment. (D) Representative images of organ fluorescence imaging after 24h. (E) Quantitative fluorescence intensities of the colon. (F) Plasma concentration time profile of free bilirubin and HA-PLGA$_{Bilirubin}$. (G) Representative fluorescence microscopy images of Rho-HA-PLGA$_{Bilirubin}$ uptake in the colon. Scale bar, 50 μm. (H) Targeted cell types in colonic tissues by Cy5.5-HA-PLGA$_{Bilirubin}$. *represents $p<0.05$, **represents $p<0.01$, ***represents $p<0.001$, ****represents $p<0.0001$.

Additionally, flow cytometry analysis (Figure 3H; Figure S12) revealed that three major types of macrophages ($CD11b^+CD11c^+$, $CD11b^+F4/80^+$, and $CD11c^+F4/80^+$ cells) exhibited uptake of Cy5.5-HA-$PLGA_{Bilirubin}$, along with dendritic cells ($CD11b^-CD11c^+$ cells; ~14.66%) and epithelial cells ($EpCAM^+$ cells; ~16.5%). In contrast, neutrophil uptake ($CD11b^+Ly6G^+$ cells) was minimal (~0.46%). Notably, in the inflamed colon of DSS-induced colitis mice, the uptake of $EpCAM^+$ cells for HA-$PLGA_{Bilirubin}$ was significantly reduced compared to the normal colon, suggesting compromised epithelial barrier integrity under colitis conditions. These findings collectively indicate that under conditions of colitis, orally administered HA-$PLGA_{Bilirubin}$ is predominantly taken up by activated macrophages in the inflamed colon exhibiting impaired epithelial barrier function.

Effective recovery of the morphology and function of the inflamed colon by HA-$PLGA_{bilirubin}$

To assess the therapeutic effect of HA-$PLGA_{bilirubin}$ against colitis, DSS-induced mice were treated with PBS, free bilirubin (30 mg/kg) and corresponding dose of various nanoparticles formulations the oral route on days 0, 2, 4 and 6 [42] (Figure 4A). Compared with PBS and other treatment groups, the DSS-induced mice given HA-$PLGA_{bilirubin}$ significantly prevented animals from bodyweight loss (Figure 4B), lower Disease Activity Index (DAI) values (Figure 4C), and shorter colon lengths (Figure 4D). Next, HE staining was used to stain colon tissue samples treated with different groups to evaluate the histological damages (Figure 4E). Compared with control health mice, DSS-induced mice showed significantly larger inflammation, characterized by depletion of goblet cells, mucosal thickening, colonic epithelium damage, inflammatory cell infiltration. Obviously, HA-$PLGA_{bilirubin}$ treatment showed significantly reduction of these inflammatory appearances than all other treatment groups and was similar to the healthy control group. Notably, histological damage of HA-PLGA-lip (empty biomaterial without bilirubin) group was similar to that in DSS-induced mice, indicating HA-$PLGA_{bilirubin}$ may exhibit their effects via increasing the accumulation of bilirubin and not HA or PLGA. DSS-induced mice treated with $PLGA_{bilirubin}$ did not reach full histological recovery, suggesting HA contributed to the retention and therapeutic efficacy of bilirubin in the inflame colon. Given that DSS-induced colitis is known to cause disruptions in intestinal tight junctions and barrier integrity, we evaluated changes in the expression of tight junction-related proteins, such as ZO-1 and Ocludin-1. Immunohistochemistry (IHC) and mRNA expression analyses were performed, and the results (Figure 4F-G) revealed significant reductions in the levels of these proteins in the colonic tissue of mice treated with PBS and HA-PLGA-lip, as expected. While bilirubin and $PLGA_{bilirubin}$ treatments demonstrated slight restoration of these proteins, the treatment with HA- $PLGA_{bilirubin}$ significantly restored the levels of ZO-1 and Ocludin-1 in the colon, bringing their protein and mRNA levels back to levels similar to those in the normal control group. In terms of intestinal permeability, we assessed this by monitoring serum fluorescence intensity following the oral administration of fluorescein isothiocyanate-labeled dextran (FITC-dextran). As anticipated, the HA-$PLGA_{bilirubin}$ treated group exhibited the lowest serum fluorescence intensity among all treatment groups (Figure 4H), indicating the lowest intestinal permeability. On the other hand, MPO level were the crucial indicators to evaluate the inflammation function repair of ulcerative colitis. As shown in Figure 4I, HA-$PLGA_{bilirubin}$ treatment decreased the level of MPO activity than other treatment (p<0.001). Together, all these findings demonstrated that HA-$PLGA_{bilirubin}$ exhibited effective recovery of the bowel's morphology and intestinal barrier function.

Promotion of colonic epithelial/stem cells regeneration after treatment with HA-$PLGA_{bilirubin}$

Modulation of epithelial proliferation/apoptosis, and stem cell regeneration were the crucial processes maintaining the homeostasis of intestine epithelial system [43, 44]. In this study, Proliferating Cell Nuclear Antigen (PCNA) and Terminal deoxynucleotidyl transferase dUTP Nick End Labeling (TUNEL) staining were used to evaluate proliferation and apoptosis of intestine epithelial cells. Compared with other treatment, HA-$PLGA_{bilirubin}$ treatment did significantly promote colonic epithelial proliferation and reduce apoptosis (Figure 5A-C). Fast-cycling $Lgr5^+$ intestinal epithelial stem cells (IESC) appear to support colonic epithelium regeneration [32], which may result in the renew and recovery of epithelium after intestinal inflammation. Herein, we used immunofluorescence staining for Lgr5 to quantify Lgr5 expression and localize $lgr5^+$IESC. As expected, DSS-induced mice and HA-PLGA-lip group both had a visible loss of IESC density in the colonic crypts (Figure 5A). Obviously, a significant higher density of $Lgr5^+$positive IESC was observed in the intestinal crypts of HA-$PLGA_{bilirubin}$ and $PLGA_{bilirubin}$ treatments compared to other groups (Figure 5D). Moreover, DSS-induced mice given HA-$PLGA_{bilirubin}$ showed a

more drastic proliferation of IESC in the colonic crypts than that of DSS-induced mice treated with $PLGA_{bilirubin}$, indicating the optimal stem cell regeneration performance of $HA\text{-}PLGA_{bilirubin}$.

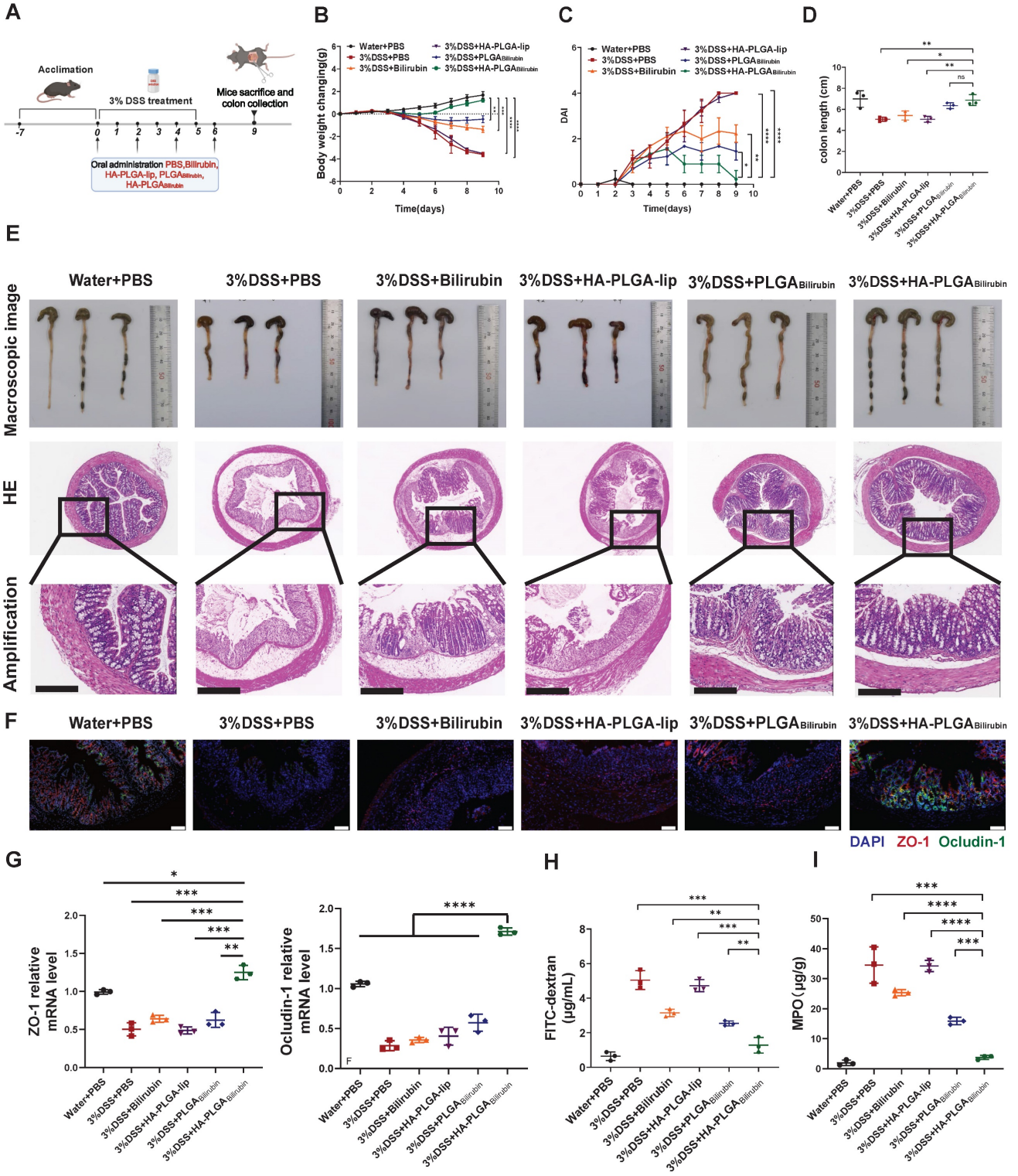

Figure 4. *In vivo* therapeutic efficacy and recovery of impaired intestinal barrier of $HA\text{-}PLGA_{bilirubin}$ in the mice with DSS-induced ulcerative colitis. (A) Schematic illustration presenting the treatment regime of the DSS-induced ulcerative colitis. Mice were fed with drinking water or drinking water containing 3% DSS for 5 days. On days 0, 2, 4, 6, mice were treated with PBS or 30 mg kg^{-1} of Bilirubin, HA-PLGA-lip (with 100K HA at equivalent mass), $PLGA_{Bilirubin}$ (with 30 mg kg^{-1} bilirubin at equivalent mass), $HA\text{-}PLGA_{Bilirubin}$ (with 100K HA and 30 mg kg^{-1} bilirubin at equivalent mass) and mice were subsequently sacrificed at day 9. (B) Body weight changes of the mice for 9 days. (C) Disease activity index (DAI) of the mice for 9 days. (D) Statistic colon length at day 9. (E) The representative microscopic and the representative HE staining image of colon tissue after various treatment. Scale bar, 250 μm. (F) Fluorescence microscopy depicting the expression levels of ZO-1 and Ocludin-1 in the colon tissues. Scale bar, 100 μm. (G) mRNA expression levels of ZO-1 and Ocludin-1 in colon tissues. (H) FITC-dextran assay for measuring intestinal permeability. (I) MPO level in the colon tissues after various treatment. *represents $p<0.05$, **represents $p<0.01$, ***represents $p<0.001$, ****represents $p<0.0001$. ns: not statistically.

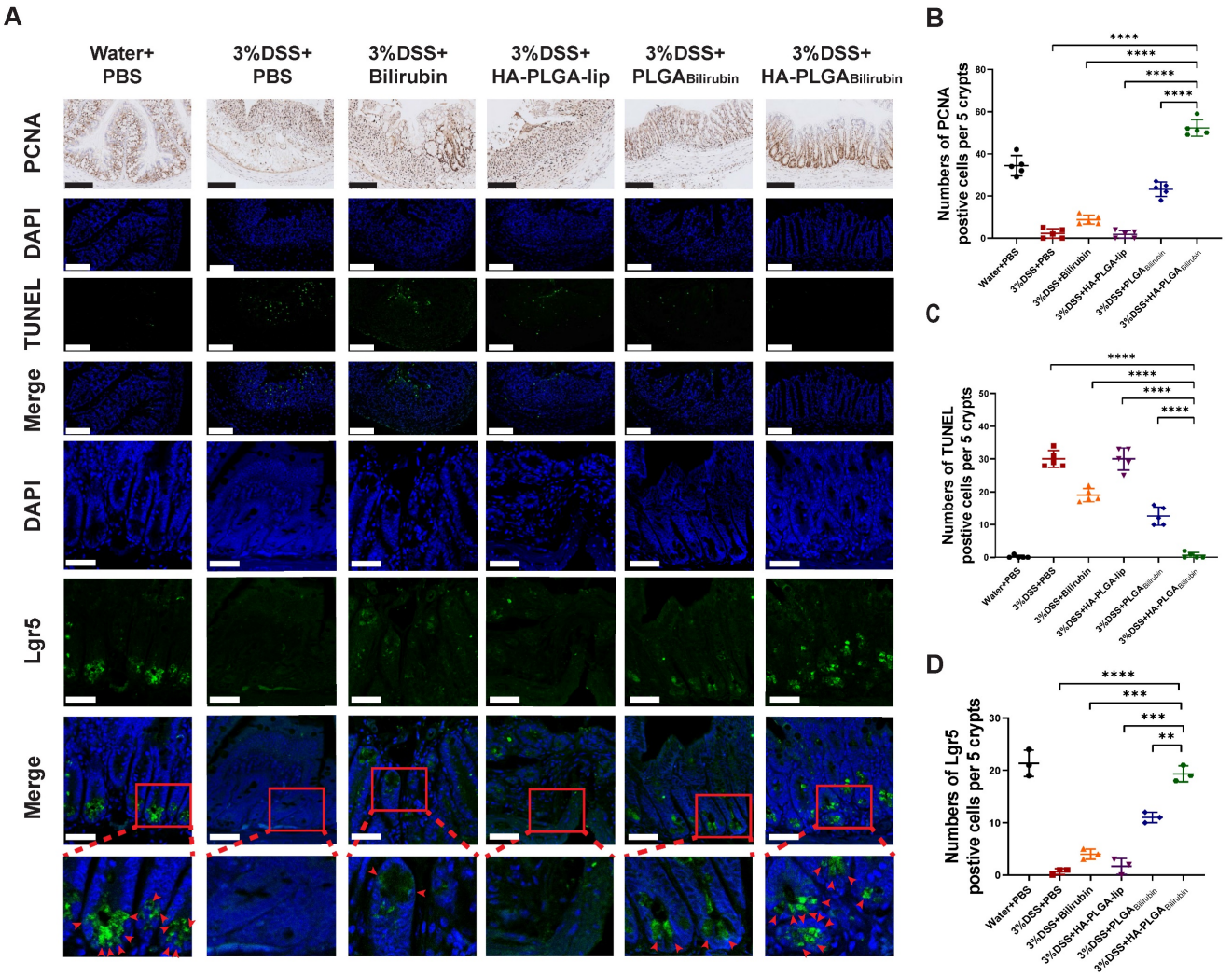

Figure 5. Effects of HA-PLGA$_{bilirubin}$ on inflamed colon cell proliferation, apoptosis and stem cell regeneration. (A) Representative Immunohistochemical images for PCNA staining (Scale bar, 140 μm), and the representative immunofluorescence images for TUNEL staining (Scale bar, 140 μm) and Lgr5 staining (Scale bar, 50 μm). (B) Quantitative analysis of the immunohistochemical staining of PCNA. (C) Quantitative analysis of the immunofluorescence staining of TUNEL. (D) Quantification of Lgr5 immunofluorescent staining. *represents $p<0.05$, **represents $p<0.01$, ***represents $p<0.001$, ****represents $p<0.0001$.

Alleviation of the angiogenesis and inflammation after treatment with HA-PLGA$_{bilirubin}$

Massive angiogenesis cascade strongly correlated with the progression of experimental colitis [45]. Herein, the reduction of angiogenesis was assessed by CD31 (an endothelial marker) staining and vascular endothelial growth factor A (VEGF-A) expression level. As shown in Figure 6A, the amount of CD31 positive cells in inflamed mucosa of DSS-induced mice was significantly higher than in control healthy mice, which is consistent with previous study [45]. Conversely, HA-PLGA$_{bilirubin}$ treatment significantly decreased the mean vessel density and area, as well as VEGF-A level (Figure 6B-C) in the colon mucosa than that of PLGA$_{bilirubin}$ treatment. On the other hand, Enzyme-Linked Immunosorbent Assay (ELISA) method was used to determine inflammatory factors measurement of tissue homogenate. HA-PLGA$_{bilirubin}$ treatment significantly increased the level of anti-inflammatory cytokines of Transforming Growth Factor Beta (TGF-β) and Interleukin-4 (IL-4) (Figure 6D-E), and reduce the level of pro-inflammatory cytokines of IL-1β (Figure 6F), IL-6 (Figure 6G), TNF-α (Figure 6H) compared to DSS-induced mice and HA-PLGA-lip. Among three bilirubin formulations, HA-PLGA$_{bilirubin}$ treatment displayed the most obvious amelioration on inflammation and angiogenesis, suggesting that the assembly of HA and PLGA could enhance the potential effect of bilirubin on DSS-induced colitis.

HA-PLGA$_{bilirubin}$ treatment reprograms transcriptional landscape *in vivo*

To further demonstrate the recovery mechanism of HA-PLGA$_{bilirubin}$ *in vivo*, colon tissues were harvested from control healthy mice and DSS-induced

mice treated with PBS, $PLGA_{bilirubin}$, $HA\text{-}PLGA_{bilirubin}$ for "transcriptomic analyses. A total of 1,969 genes was differentially expressed between DSS-induced mices given PBS and $HA\text{-}PLGA_{bilirubin}$ (p_{adjust}<0.05, |log2FoldChange| ≥ 2), of which 818 genes were upregulated and 1,151 genes were downregulated (Figure 7A). Significant differences existed between the groups in terms of the expression level of these 1,969 genes (Figure S13A). Gene Ontology (GO) enrichment analysis showed that these Differentially Expressed Genes (DEGs) were mainly involved in the regulation of inflammatory response, regulation of epithelial cell proliferation, defense response to bacterium, regulation of innate immune response, and regulation of apoptotic signaling pathway (Figure 7B). In the Kyoto Encyclopedia of Genes and Genomes (KEGG) pathway analysis, enriched pathways and diseases included inflammatory bowel disease (IBD), TNF-signaling pathway, and IL-17 signaling pathway (Figure 7C; Figure S13B--C). More specifically, upregulated genes were mainly associated with the metabolism modulation, including fatty acid metabolic process, retinol metabolism, and acid metabolism (Figure S14A-B).

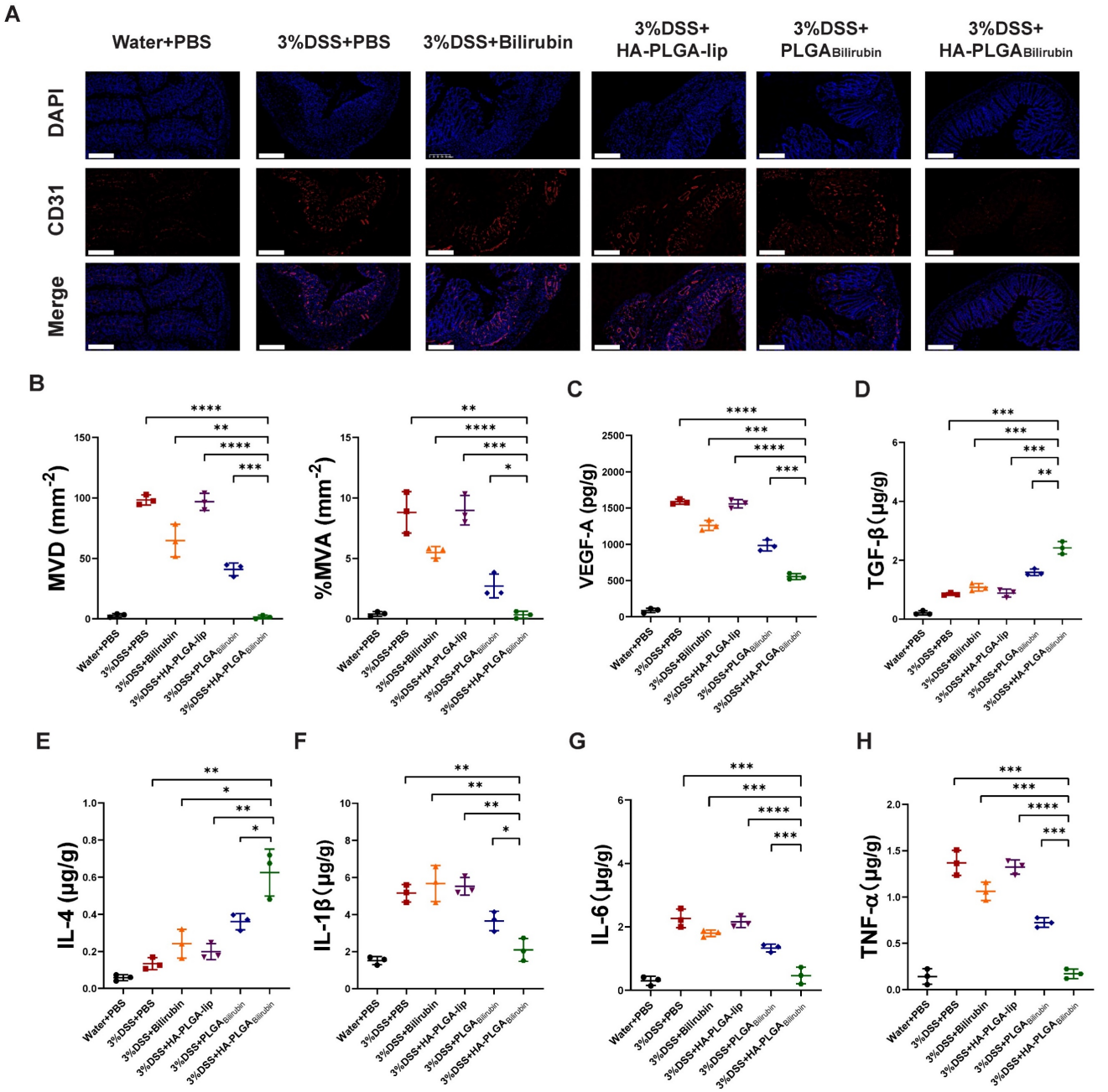

Figure 6. $HA\text{-}PLGA_{bilirubin}$ against ulcerative colitis via alleviating angiogenesis and inflammation of inflamed colon. (A) Representative immunofluorescence images for CD31 staining after various treatment. Scale bar, 240 μm. (B) The mean vessel density (MVD) and mean vessel area/mm² (MVA) of mucosa were quantified. (C) VEGF-A level in the colon tissues after various treatment. (D, E, F, G, H) Inflammatory factor level of TGF-β (D), IL-4 (E), IL-1β (F), IL6 (G), and TNF-α (H) in the colon tissues after various treatment. *represents p<0.05, **represents p<0.01, ***represents p<0.001, ****represents p<0.0001.

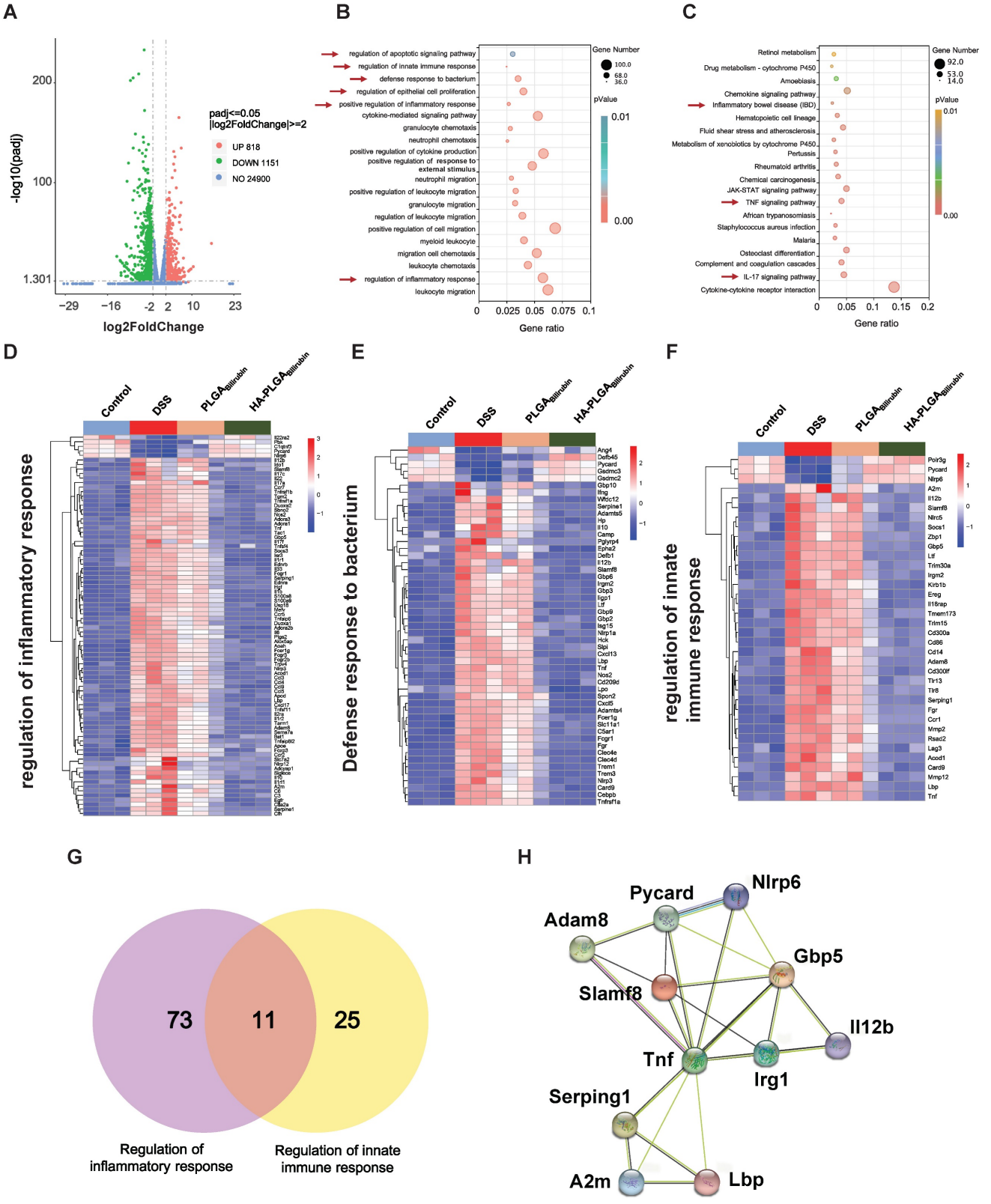

Figure 7. Transcriptomic analysis of the colon tissues. (A) A Volcano plot presenting the significantly differentially expressed genes (p<0.05 and |Log_2 Fold change| ≥2) between DSS+HA-PLGA$_{bilirubin}$ group compared to the DSS group, including 818 upregulated genes and 1,151 downregulated genes. (B, C) GO enrichment analysis (B) and KEGG pathway analysis (C) of the significantly differentially expressed genes. (D, E, F) The heatmap of differentially expressed genes associated with regulation of inflammatory response (D), defense response to bacterium (E) and regulation of innate immune response (F). (G) Venn diagram of the differentially expressed genes between comparisons. 11 genes regulate both regulation of inflammatory response and regulation of innate immune response. (H) Functional association networks of the co-expressed genes that allow the simultaneous regulation of both regulation of inflammatory response and regulation of innate immune response.

The downregulated genes were mainly involved in the regulation of inflammatory response, positive regulation of defense response, Toll-like receptor signaling pathway, and NOD-like receptor signaling pathway, which played a key role in the inflammatory and immune responses (Figure S14C-D). Moreover, we further analyzed the function of innate immunity and host defense-related genes, and gene set with specific functions of each group indicated that regulation of inflammatory response-related genes (Figure 7D), defense response to bacterium-related genes (Figure 7E), and regulation of innate immune response-related genes (Figure 7F) were obviously downregulated in HA-PLGA$_{bilirubin}$ treatment. As inflammation and immune regulation are highly associated with UC recovery [46], we obtained 11 genes that participated in the regulation of inflammatory response and regulation of innate immune response together after HA-PLGA$_{bilirubin}$ treatment (Figure 7G). A PPI analysis revealed significantly enriched interactions between those genes (Figure 7H). Furthermore, we have included Western blot experiments to investigate the expression levels of key proteins involved in the TNF and Interleukin-17 (IL-17) signaling pathways, such as TNF-α and IL-17A, providing additional evidence for the therapeutic role of HA-PLGA$_{Bilirubin}$ hydrogels. Our results show that TNF-α and IL-17A protein levels are significantly increased during the inflammatory process, and HA-PLGA$_{Bilirubin}$ hydrogels can significantly reduce the expression of these two proteins (Figure S15), indicating that HA-PLGA$_{Bilirubin}$ hydrogel may repair DSS-induced colitis by negatively regulating the TNF and IL-17 signaling pathways. Together, HA-PLGA$_{bilirubin}$ treatment significantly elicit a regulation of inflammatory response and innate immune response to repair DSS-induced colitis.

Discussion

To our knowledge, our study is the first attempt to combine the pH-responsive hydrogels with HA-based bilirubin for the dual-targeting treatment of UC. Compared with previous studies which suffer from HA's susceptibility to diffusion or degradation in digestive juice [18, 19], our proposed nanoparticles overcome these dilemmas, and dramatically improve the release and accumulation of bilirubin at the inflammatory location of UC through pH-responsive reaction and HA-targeted inflammatory macrophages mechanism. Moreover, our *in vivo* experiments support the potent therapeutic efficacy of HA-PLGA$_{bilirubin}$ and show some novel recovery mechanisms associated with intestinal epithelial/stem cell regeneration and immune response modulation capabilities.

The study has certain strengths. First, we have enhanced the oral applicability of traditional HA-bilirubin nanoparticles by introducing pH-responsive hydrogels. In the previous study, Lee et al. and Huang et al. have designed HA-bilirubin nanoparticles through amphiphilic conjugation effects between HA and bilirubin [18] or self-assembly of ε-polylysine-bilirubin and HA [19]. However, HA-based nanoparticles may suffer from their uncontrollable systemic diffusion and adverse systemic effects during oral administration delivery to treat colon disease [47]. To eliminate the impact of HA, we embedded them into a pH-responsive hydrogel, and this binding may protect the HA-based bilirubin from premature degradation and bursting release by gastric proteolytic enzymes. As expected, our study showed that hydrogels may not only protect HA-based bilirubin from premature degradation by gastric enzymes, but also allows HA-based bilirubin to be targeted to specific sites in the gastrointestinal tract without premature release. Therefore, combination of hydrogels and HA-bilirubin nanoparticles may be a highly effective approach for accelerating the healing process of ulcers in UC mice.

Second, we further investigated and observed the therapeutic effects and mechanisms of HA-PLGA$_{bilirubin}$ hydrogels in UC. Previous studies have reported that bilirubin exerts antioxidative, anti-inflammatory, and immunoregulatory effects against various inflammatory diseases [16, 48-50]. However, these studies on the mechanisms underlying the therapeutic effects of bilirubin in UC have been relatively superficial and require to be further clarified. In our experiments, the prepared bilirubin nanoparticles were found to be able to repair damaged colon in UC with the superior therapeutic effects compared to bilirubin therapy alone. Further experiments revealed that such beneficial effects were associated with the modulation of intestinal epithelial/stem cells regeneration and decreasing of angiogenesis and inflammation. In particular, this is also the first demonstration that HA-PLGA$_{bilirubin}$ treatment can ameliorate DSS-induced colitis by modulating colonic epithelial/stem cells regeneration, which extends our knowledge on the therapeutic mechanisms of bilirubin [51-53]. By shedding light on this innovative area of research, our findings may pave the way for the development of bilirubin for the treatment of chronic inflammatory conditions.

At last, we explored the potential immune mechanism of HA-PLGA$_{bilirubin}$ hydrogels in recovering mucosal damage in UC. Previous studies indicated that innate immune responses played a vital role in the development and protection of UC [54-58].

Similarly, we uncovered the significant alteration of innate immune responses before and after HA-PLGA$_{bilirubin}$ treatment using transcriptome profiling [59]. This alteration was especially related to TNF and IL-17 signaling pathway, which have been reported to be critically involved in the pathogenesis of various inflammatory disorders including UC [60-62]. Herein, our findings demonstrated that HA-PLGA$_{bilirubin}$ hydrogels may play a therapeutic role by modulation of innate immune responses especially negative regulation of TNF and IL-17 signaling pathway. As UC is a polygenic disease related to immunodeficiency [63, 64], we further screened 11 genes including TNF that interact with it, which may provide potential targets of intervention for UC.

Conclusions

To sum up, our work developed a novel bilirubin delivery system that formed by hydrogel encapsulating hyaluronic acid (HA)-functionalized PLGA/liposome nanoparticles (HA-PLGA$_{bilirubin}$). The prepared nanoparticles exhibit potent pH-responsive delivery and HA-targeting functions, which enhances the repair effects of bilirubin via modulation of intestinal epithelial/stem cells regeneration and immune response. It is envisaged that this study will provide a safe and promising oral drug delivery system for the treatment of ulcerative colitis.

Supplementary Material

Supplementary figures and table.
https://www.thno.org/v14p0528s1.pdf

Acknowledgements

This work was funded by the National Natural Science Foundation of China Regional Innovation and Development Joint Foundation (U23A20408), National Natural Science Foundation of China (82171698, 82170561, 81300279, 81741067), the Natural Science Foundation for Distinguished Young Scholars of Guangdong Province (2021B1515020003), Project to Attract Foreign Experts from Minister of Science and Technology of China (G2022030047L), Natural Science Foundation of Guangdong Province (2022A15150 12081), the Foreign Distinguished Teacher Program of Guangdong Science and Technology Department (KD0120220129), the Climbing Program of Introduced Talents and High-level Hospital Construction Project of Guangdong Provincial People's Hospital (DFJH 201803, KJ012019099, KJ012021143, KY012021183).

Author contributions

ZWZ, KHG, YJL, and QY analyzed and organized the data; ZWZ wrote this manuscript; ZWZ, HHW, RJZ, RJ, JWL, and RW generated the figure and tables; HC, YLF, WHS, and QZL designed, revised and supervised the study. All authors reviewed and approved the final manuscript.

Data availability

All data included in this study are available upon request by contact with the corresponding author.

Competing Interests

The authors have declared that no competing interest exists.

References

1. Hoie O, Wolters F, Riis L, Aamodt G, Solberg C, Bernklev T, et al. Ulcerative colitis: patient characteristics may predict 10-yr disease recurrence in a European-wide population-based cohort. Am J Gastroenterol. 2007; 102: 1692-701.
2. Park SH, Park-Min KH, Chen J, Hu X, Ivashkiv LB. Tumor necrosis factor induces GSK3 kinase-mediated cross-tolerance to endotoxin in macrophages. Nat Immunol. 2011; 12: 607-15.
3. Stagg AJ, Hart AL, Knight SC, Kamm MA. The dendritic cell: its role in intestinal inflammation and relationship with gut bacteria. Gut. 2003; 52: 1522-9.
4. Cao F, Jin L, Gao Y, Ding Y, Wen H, Qian Z, et al. Artificial-enzymes-armed Bifidobacterium longum probiotics for alleviating intestinal inflammation and microbiota dysbiosis. Nat Nanotechnol. 2023; 18: 617-27.
5. Bernstein CN, Fried M, Krabshuis JH, Cohen H, Eliakim R, Fedail S, et al. World Gastroenterology Organization Practice Guidelines for the diagnosis and management of IBD in 2010. Inflamm Bowel Dis. 2010; 16: 112-24.
6. Stallmach A, Hagel S, Bruns T. Adverse effects of biologics used for treating IBD. Best Pract Res Clin Gastroenterol. 2010; 24: 167-82.
7. Aggarwal A, Sabol T, Vaziri H. Update on the Use of Biologic Therapy in Ulcerative Colitis. Curr Treat Options Gastroenterol. 2017; 15: 155-67.
8. Hammerman C, Goldschmidt D, Caplan MS, Kaplan M, Bromiker R, Eidelman AI, et al. Protective effect of bilirubin in ischemia-reperfusion injury in the rat intestine. J Pediatr Gastroenterol Nutr. 2002; 35: 344-9.
9. Stocker R, Yamamoto Y, McDonagh AF, Glazer AN, Ames BN. Bilirubin is an antioxidant of possible physiological importance. Science. 1987; 235: 1043-6.
10. Ceran C, Sonmez K, Turkyllmaz Z, Demirogullarl B, Dursun A, Duzgun E, et al. Effect of bilirubin in ischemia/reperfusion injury on rat small intestine. J Pediatr Surg. 2001; 36: 1764-7.
11. Perlstein TS, Pande RL, Creager MA, Weuve J, Beckman JA. Serum total bilirubin level, prevalent stroke, and stroke outcomes: NHANES 1999-2004. Am J Med. 2008; 121: 781-8 e1.
12. Otani K, Shimizu S, Chijiiwa K, Morisaki T, Yamaguchi T, Yamaguchi K, et al. Administration of bacterial lipopolysaccharide to rats induces heme oxygenase-1 and formation of antioxidant bilirubin in the intestinal mucosa. Dig Dis Sci. 2000; 45: 2313-9.
13. Ryter SW, Alam J, Choi AM. Heme oxygenase-1/carbon monoxide: from basic science to therapeutic applications. Physiol Rev. 2006; 86: 583-650.
14. Vogel ME, Zucker SD. Bilirubin acts as an endogenous regulator of inflammation by disrupting adhesion molecule-mediated leukocyte migration. Inflamm Cell Signal. 2016; 3.
15. Zucker SD, Vogel ME, Kindel TL, Smith DL, Idelman G, Avissar U, et al. Bilirubin prevents acute DSS-induced colitis by inhibiting leukocyte infiltration and suppressing upregulation of inducible nitric oxide synthase. Am J Physiol Gastrointest Liver Physiol. 2015; 309: G841-54.
16. Longhi MS, Vuerich M, Kalbasi A, Kenison JE, Yeste A, Csizmadia E, et al. Bilirubin suppresses Th17 immunity in colitis by upregulating CD39. JCI Insight. 2017; 2.
17. Julka K, Ko CW. Infectious diseases and the gallbladder. Infect Dis Clin North Am. 2010; 24: 885-98, vii-viii.
18. Lee Y, Sugihara K, Gillilland MG, 3rd, Jon S, Kamada N, Moon JJ. Hyaluronic acid-bilirubin nanomedicine for targeted modulation of dysregulated intestinal barrier, microbiome and immune responses in colitis. Nat Mater. 2020; 19: 118-26.
19. Huang ZW, Shi Y, Zhai YY, Du CC, Zhai J, Yu RJ, et al. Hyaluronic acid coated bilirubin nanoparticles attenuate ischemia reperfusion-induced acute kidney injury. J Control Release. 2021; 334: 275-89.
20. Zeeshan M, Ali H, Khan S, Khan SA, Weigmann B. Advances in orally-delivered pH-sensitive nanocarrier systems; an optimistic approach for the treatment of inflammatory bowel disease. Int J Pharm. 2019; 558: 201-14.
21. Liu P, Gao C, Chen H, Vong CT, Wu X, Tang X, et al. Receptor-mediated targeted drug delivery systems for treatment of inflammatory bowel disease: Opportunities and emerging strategies. Acta Pharm Sin B. 2021; 11: 2798-818.

22. Daugherty AL, Mrsny RJ. Transcellular uptake mechanisms of the intestinal epithelial barrier Part one. Pharm Sci Technol Today. 1999; 4: 144-51.
23. Chen Z, Wang Z, Gu Z. Bioinspired and Biomimetic Nanomedicines. Acc Chem Res. 2019; 52: 1255-64.
24. Ma Y, Duan L, Sun J, Gou S, Chen F, Liang Y, et al. Oral nanotherapeutics based on Antheraea pernyi silk fibroin for synergistic treatment of ulcerative colitis. Biomaterials. 2022; 282: 121410.
25. Ma Y, Bjornmalm M, Wise AK, Cortez-Jugo C, Revalor E, Ju Y, et al. Gel-Mediated Electrospray Assembly of Silica Supraparticles for Sustained Drug Delivery. ACS Appl Mater Interfaces. 2018; 10: 31019-31.
26. Kotla NG, Gulati M, Singh SK, Shivapooja A. Facts, fallacies and future of dissolution testing of polysaccharide based colon-specific drug delivery. J Control Release. 2014; 178: 55-62.
27. de Vos S, Swinnen LJ, Wang D, Reid E, Fowler N, Cordero J, et al. Venetoclax, bendamustine, and rituximab in patients with relapsed or refractory NHL: a phase Ib dose-finding study. Ann Oncol. 2018; 29: 1932-8.
28. Shao M, Vishvanath L, Busbuso NC, Hepler C, Shan B, Sharma AX, et al. De novo adipocyte differentiation from Pdgfrbeta(+) preadipocytes protects against pathologic visceral adipose expansion in obesity. Nat Commun. 2018; 9: 890.
29. Chen H, Zhang H, Zheng Y, Min X, Luo Y, Zhou W, et al. Prolyl hydroxylase 2 silencing enhances the paracrine effects of mesenchymal stem cells on necrotizing enterocolitis in an NF-kappaB-dependent mechanism. Cell Death Dis. 2020; 11: 188.
30. Chen H, Min XH, Wang QY, Leung FW, Shi L, Zhou Y, et al. Pre-activation of mesenchymal stem cells with TNF-alpha, IL-1beta and nitric oxide enhances its paracrine effects on radiation-induced intestinal injury. Sci Rep. 2015; 5: 8718.
31. Yang D, Chen Y, Peng H, Chen G, Lin Z. An integrated experimental and theoretical study on the optical properties of uniform hairy noble metal nanoparticles. Nanoscale. 2018; 10: 22750-7.
32. Lv S, Du Y, Wu F, Cai Y, Zhou T. Review on LSPR assisted photocatalysis: effects of physical fields and opportunities in multifield decoupling. Nanoscale Adv. 2022; 4: 2608-31.
33. Guo Q, Jiang C. Delivery strategies for macromolecular drugs in cancer therapy. Acta Pharm Sin B. 2020; 10: 979-86.
34. Zhang L, Wu S, Qin Y, Fan F, Zhang Z, Huang C, et al. Targeted Codelivery of an Antigen and Dual Agonists by Hybrid Nanoparticles for Enhanced Cancer Immunotherapy. Nano Lett. 2019; 19: 4237-49.
35. Lu C, Stewart DJ, Lee JJ, Ji L, Ramesh R, Jayachandran G, et al. Phase I clinical trial of systemically administered TUSC2(FUS1)-nanoparticles mediating functional gene transfer in humans. PLoS One. 2012; 7: e34833.
36. Porteous DJ, Dorin JR, McLachlan G, Davidson-Smith H, Davidson H, Stevenson BJ, et al. Evidence for safety and efficacy of DOTAP cationic liposome mediated CFTR gene transfer to the nasal epithelium of patients with cystic fibrosis. Gene Ther. 1997; 4: 210-8.
37. Lv H, Zhang S, Wang B, Cui S, Yan J. Toxicity of cationic lipids and cationic polymers in gene delivery. J Control Release. 2006; 114: 100-9.
38. Zhang BF, Xing L, Qiao JB, Cui PF, Wang FZ, Zhang JL, et al. In vivo synergistic antitumor effect and safety of siRNA and lonidamine dual-loaded hierarchical targeted nanoparticles. Int J Pharm. 2016; 506: 207-13.
39. Duan X, Zhang Y, Guo M, Fan N, Chen K, Qin S, et al. Sodium alginate coating simultaneously increases the biosafety and immunotherapeutic activity of the cationic mRNA nanovaccine. Acta Pharm Sin B. 2023; 13: 942-54.
40. Reid SD, Pockley AG. Cytokine regulation of CD44 expression on rat intestinal epithelial cells. Immunol Invest. 2000; 29: 271-86.
41. Almalik A, Karimi S, Ouasti S, Donno R, Wandrey C, Day PJ, et al. Hyaluronic acid (HA) presentation as a tool to modulate and control the receptor-mediated uptake of HA-coated nanoparticles. Biomaterials. 2013; 34: 5369-80.
42. Kotla NG, Singh R, Baby BV, Rasala S, Rasool J, Hynes SO, et al. Inflammation-specific targeted carriers for local drug delivery to inflammatory bowel disease. Biomaterials. 2022; 281: 121364.
43. Tessner TG, Cohn SM, Schloemann S, Stenson WF. Prostaglandins prevent decreased epithelial cell proliferation associated with dextran sodium sulfate injury in mice. Gastroenterology. 1998; 115: 874-82.
44. Danese S, Sans M, de la Motte C, Graziani C, West G, Phillips MH, et al. Angiogenesis as a novel component of inflammatory bowel disease pathogenesis. Gastroenterology. 2006; 130: 2060-73.
45. Zhao YZ, ZhuGe DL, Tong MQ, Lin MT, Zheng YW, Jiang X, et al. Ulcerative colitis-specific delivery of keratinocyte growth factor by neutrophils-simulated liposomes facilitates the morphologic and functional recovery of the damaged colon through alleviating the inflammation. J Control Release. 2019; 299: 90-106.
46. Bakhautdin B, Febbraio M, Goksoy E, de la Motte CA, Gulen MF, Childers EP, et al. Protective role of macrophage-derived ceruloplasmin in inflammatory bowel disease. Gut. 2013; 62: 209-19.
47. Liu H, Cai Z, Wang F, Hong L, Deng L, Zhong J, et al. Colon-Targeted Adhesive Hydrogel Microsphere for Regulation of Gut Immunity and Flora. Adv Sci (Weinh). 2021; 8: e2101619.
48. Hou S, Reynolds MF, Horrigan FT, Heinemann SH, Hoshi T. Reversible binding of heme to proteins in cellular signal transduction. Acc Chem Res. 2006; 39: 918-24.
49. Kapitulnik J. Bilirubin: an endogenous product of heme degradation with both cytotoxic and cytoprotective properties. Mol Pharmacol. 2004; 66: 773-9.
50. Sedlak TW, Saleh M, Higginson DS, Paul BD, Juluri KR, Snyder SH. Bilirubin and glutathione have complementary antioxidant and cytoprotective roles. Proc Natl Acad Sci U S A. 2009; 106: 5171-6.
51. Wang WW, Smith DL, Zucker SD. Bilirubin inhibits iNOS expression and NO production in response to endotoxin in rats. Hepatology. 2004; 40: 424-33.
52. Gou S, Huang Y, Wan Y, Ma Y, Zhou X, Tong X, et al. Multi-bioresponsive silk fibroin-based nanoparticles with on-demand cytoplasmic drug release capacity for CD44-targeted alleviation of ulcerative colitis. Biomaterials. 2019; 212: 39-54.
53. Chen R, Lin X, Wang Q, An X, Zhao X, Lin Y, et al. Dual-targeting celecoxib nanoparticles protect intestinal epithelium and regulate macrophage polarization for ulcerative colitis treatment. Chemical Engineering Journal. 2023; 452: 139445.
54. Zenewicz LA, Yancopoulos GD, Valenzuela DM, Murphy AJ, Stevens S, Flavell RA. Innate and adaptive interleukin-22 protects mice from inflammatory bowel disease. Immunity. 2008; 29: 947-57.
55. Watanabe T, Kitani A, Murray PJ, Wakatsuki Y, Fuss IJ, Strober W. Nucleotide binding oligomerization domain 2 deficiency leads to dysregulated TLR2 signaling and induction of antigen-specific colitis. Immunity. 2006; 25: 473-85.
56. Li H, Fan C, Lu H, Feng C, He P, Yang X, et al. Protective role of berberine on ulcerative colitis through modulating enteric glial cells-intestinal epithelial cells-immune cells interactions. Acta Pharm Sin B. 2020; 10: 447-61.
57. Tong L, Hao H, Zhang Z, Lv Y, Liang X, Liu Q, et al. Milk-derived extracellular vesicles alleviate ulcerative colitis by regulating the gut immunity and reshaping the gut microbiota. Theranostics. 2021; 11: 8570-86.
58. Rahman AT, Shin J, Whang CH, Jung W, Yoo D, Seo C, et al. Bilirubin Nanomedicine Rescues Intestinal Barrier Destruction and Restores Mucosal Immunity in Colitis. ACS Nano. 2023; 17: 10996-1013.
59. Jin L, Cao F, Gao Y, Zhang C, Qian Z, Zhang J, et al. Microenvironment-Activated Nanozyme-Armed Bacteriophages Efficiently Combat Bacterial Infection. Adv Mater. 2023; 35: e2301349.
60. Grabinger T, Bode KJ, Demgenski J, Seitz C, Delgado ME, Kostadinova F, et al. Inhibitor of Apoptosis Protein-1 Regulates Tumor Necrosis Factor-Mediated Destruction of Intestinal Epithelial Cells. Gastroenterology. 2017; 152: 867-79.
61. O'Connor W, Jr., Kamanaka M, Booth CJ, Town T, Nakae S, Iwakura Y, et al. A protective function for interleukin 17A in T cell-mediated intestinal inflammation. Nat Immunol. 2009; 10: 603-9.
62. Zhu S, Pan W, Shi P, Gao H, Zhao F, Song X, et al. Modulation of experimental autoimmune encephalomyelitis through TRAF3-mediated suppression of interleukin 17 receptor signaling. J Exp Med. 2010; 207: 2647-62.
63. Anderson CA, Massey DC, Barrett JC, Prescott NJ, Tremelling M, Fisher SA, et al. Investigation of Crohn's disease risk loci in ulcerative colitis further defines their molecular relationship. Gastroenterology. 2009; 136: 523-9 e3.
64. Uhlig HH. Monogenic diseases associated with intestinal inflammation: implications for the understanding of inflammatory bowel disease. Gut. 2013; 62: 1795-805.